Heteromeric assembly of the *human ether-a-go-go* related gene (hERG) channel: a heterologous expression system for assessing type II Long QT syndrome causing mutations

John Read

Department of Biochemistry

McGill University

Montréal, Québec, Canada

January 2023

A thesis submitted to McGill University in partial fulfillment of the requirements of the degree of Master of Science in Biochemistry

Table of Contents

Abstract

The human Ether-a-go-go related gene (hERG) ion channel is a key regulator of cardiac membrane repolarization, and its dysfunction causes Long QT syndrome type 2 (LQT2), a common yet uncurable congenital disorder. LQT2 significantly increases a patient's risk of severe heart disease, including arrhythmia and sudden death.

hERG is a heterotetramer composed of four subunits of two isoforms of the gene: hERG1a, which is the full-length protein, and hERG1b which lacks most of the N-terminus, including the PAS domain, key to the channel's gating kinetics. LQT2 is autosomal dominant, meaning patients have a single mutant allele, however the molecular mechanisms related to the mutations remain poorly characterized. Most mutations in hERG cause its misfolding, leading to retention in the endoplasmic reticulum (ER), ER-associated degradation or aggregation.

In this work, we propose two mechanisms and postulate how each is responsible for the disease. The dominant negative (DN) mechanism is the association of wild-type (WT) and mutant subunits, causing misfolding of the whole channel, while the haploinsufficiency (HI) mechanism involves a lack of association between WT and mutant subunits, resulting in an insufficient complement of hERG channels on the cell surface. To determine the extent to which these mechanisms are involved, we developed a co-expression system in HEK-293 Flp-In TREx cells wherein differentially tagged WT and mutant hERG could be inducibly co-expressed in each of their 1a and 1b isoforms. The viability of this system is validated in several assays, including surface biotinylation, co-immunoprecipitation and fluorescence microscopy.

This work is a key step in understanding the structural determinants of the DN and HI mechanisms, which will allow for the eventual prediction of disease severity based on genotype.

Resumé

Le canal ionique hERG (human Ether-a-go-go related gene) est un régulateur clé de la repolarisation de la membrane cardiaque. Son dysfonctionnement est à l'origine du syndrome du QT long de type 2 (LQT2), une maladie congénitale commune mais incurable. Le LQT2 augmente considérablement le risque de maladie cardiaque sérieuse, notamment d'arythmie et d'arrêt cardiaque.

La protéine hERG est un hétérotétramère composé de deux isoformes du gène : hERG1a, qui est la protéine complète, et hERG-1b. Il manque à cette dernière la majorité de l'extrémité N-terminale, y compris le domaine Per-Arnt-Slim (PAS), essentiel à la fonction du canal. La LQT2 est autosomique dominante, ce qui signifie que les patients ont un seul allèle mutant, mais les mécanismes moléculaires liés aux mutations restent mal connus. La plupart des mutations de l'hERG provoquent son mauvais repliement, ce qui entraîne sa rétention dans le réticulum endoplasmique (RE), sa dégradation associée au RE ou son agrégation.

Dans le cadre de ce mémoire, nous examinerons deux mécanismes et nous expliquerons comment chacun pourrait être responsable de la maladie. Le mécanisme dominant négatif (DN), lorsqu'il y a de l'association entre des monomères de type sauvage (WT) et des monomères mutantes, entraînant un mauvais repliement de l'ensemble du canal tétramérique. Au contraire, le mécanisme d'haplo-insuffisance (HI) implique une absence d'association entre les monomères WT et mutants, donc les canaux tétramériques sont constitués seulement de protéines WT. Cela entraîne un complément insuffisant de canaux hERG à la surface des cellules.

Pour déterminer dans quelle mesure ces mécanismes sont impliqués, nous avons développé un système de co-expression dans des cellules HEK-293 Flp-In TREx. Avec ce système, des canaux hERG WT et mutants marqués différemment peuvent être co-exprimés de manière inductible dans chacune de leurs isoformes 1a et 1b. La validité de ce système est vérifiée par plusieurs tests, notamment la biotinylation de surface, la co-immunoprécipitation et la microscopie à fluorescence. Un deuxième système comprenant la transfection transitoire des cellules HeLa est aussi évalué, mais n'était pas suffisamment reproductible.

Ce travail est une étape clé pour améliorer la connaissance des déterminants structurels des mécanismes DN et HI, ce qui permettra à terme de prédire la sévérité de la maladie LQT2 en fonction du génotype.

Acknowledgements

It goes without saying that none of this work would have been possible without the support of my late supervisor Dr. Jason Young. His perseverance and dedication to his students went above and beyond any expectation, before and after his diagnosis. I have not known such dedication to his work. He was an amazing teacher and mentor, and I am honoured to have had him as a part of my life. May he rest in peace.

Thank you to Jason's lab members. Particularly Michael Wong: for the training you provided on most lab techniques, and our frequent philosophical debates which kept me sane throughout the COVID-19 pandemic. I still do not believe it is possible to know if I am the same person I was then, or if I am a copy. I hope your new lab is treating you well.

A big thank you to Alvin Shrier for providing the expertise on hERG and picking up as my primary mentor where Jason left off. Your positivity and support throughout these tumultuous couple years has been invaluable. Thank you to David Thomas for providing a work area in the final months of my degree. Likewise, David's lab, notably Graeme Carlile and Kurt Dejgaard, who provided much needed technical help.

Thank you to my committee members Dr's Kalle Gehring and John Orlowski, as well as Dr. Gergely Lukacs providing valuable criticisms and suggestions relating to my experiments.

Finally, I'd like to thank my girlfriend Marie-Pier for helping me with the translation of my abstract, for her moral support throughout this degree, and for tolerating my erratic schedule with occasional diversions to the lab at odd hours. I couldn't have finished this without you.

List of abbreviations[1]

Acronym	Meaning
ATP	adenosine triphosphate
Cas9	CRISPR-associated protein 9
CFTR	cystic fibrosis transmembrane conductance regulator
CG	core glycosylation
CHIP	C-terminus of Hsc70-interacting protein
CM	cardiomyocyte
CMV	cytomegalovirus
CNBHD	cyclic nucleotide binding homology domain
CRISPR	clustered regularly interspaced short palindromic repeats
cryo-EM	cryo-electron microscopy
CVD	Cardiovascular disease
DJA1	DNAJA1 (same pattern for other DNAJ proteins)
DN	Dominant negative
DNA	deoxyribonucleic acid
ECG	electrocardiogram
ER	endoplasmic reticulum
ERAD	endoplasmic reticulum associated degradation
FDA	food and drug administration
FG	full glycosylation
Flp-in	Flippase integration
HA	hemagglutinin
hERG	Human ether-a-go-go related gene
HI	Haploinsufficient
HOP	Hsp70-Hsp90 organizing protein
Hsp70	Heat shock protein 70 kDa
Hsp90	Heat shock protein 90 kDa
IP	Immunoprecipitation
iPSC	induced pluripotent stem cells
LQT2	Long QT syndrome type 2
LQTS	Long QT syndrome
mRNA	messenger RNA
MVB	multi-vesicular body
PAS	Per-Arnt-Sim domain
PC	patch clamp

[1] Abbreviations for specific constructs used in experiments are shown in Table II (page 64)

PM	plasma membrane
poly-Ub	poly-Ubiquitination
PTM	post-translational modification
Q4	KCNQ4 ion channel
QC	quality control
SC	stem cell
TREx	tetracycline-regulated expression
WT	wild-type

Contributions of Authors

All experiments shown in this work were performed and analyzed by John Read. Experimental design and data analysis were conducted by John Read, with the assistance of Jason Young and Alvin Shrier.

Contribution to Original Knowledge

Despite being a heteromeric channel, previous studies have not studied mutant hERG channels comparing mutants expressed as both 1a and 1b isoforms. In this work, we develop an expression system and several assays to study LQT2-causing mutants. Focusing on the G601S mutant, we highlight differences between 1a and 1b G601S.

Introduction

1: The Cardiac Action Potential

Cardiovascular disease (CVD) is the second leading cause of death in Canada (after cancer), as well as being the costliest form of illness to treat(1). But the lethality and healthcare costs do not fully describe its impact: for people who do survive heart failure, the decrease in quality of life and loss in economic productivity is substantial. Combined, these were estimated in 2009 to cost the Canadian economy over $22 billion per year (1). CVD is a broad category, with some forms caused primarily by environmental factors (diet, drugs), while others are congenital (structural/functional mutations in the genes) (2). Most of these result in improper heart function.

The heart contracts and relaxes to pump blood through the body in a controlled manner. This is mediated by cardiomyocytes which initiate and conduct action potentials that are generated by movement of potassium, calcium and sodium ions across the cell membrane

through ion channels (3). Each channel plays a specific role in maintaining the cycle, thus dysfunction of any one channel can throw the cycle into disarray and lead to cardiac arrhythmias (3).

a

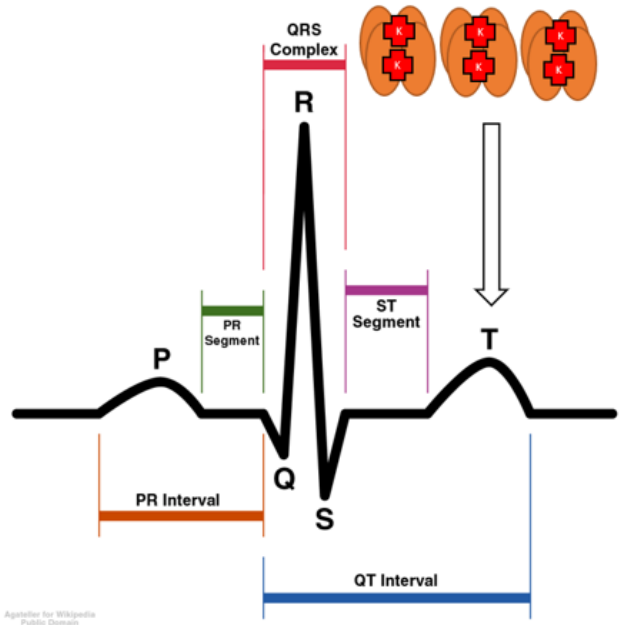

b

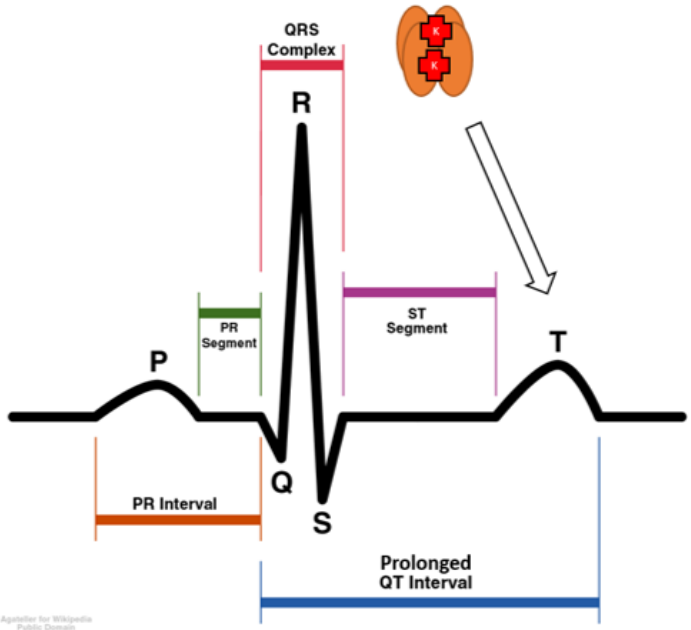

c

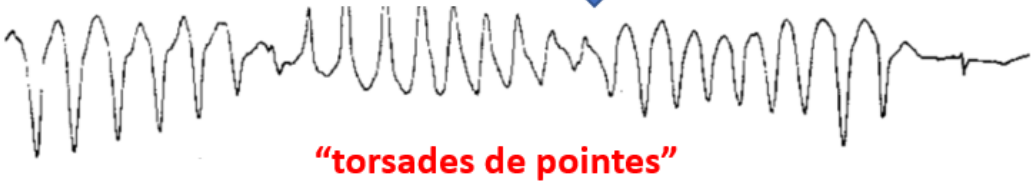

"torsades de pointes"

Figure 1: Delayed repolarization of the ventricular action potential prolongs the QT interval of the ECG and causes "torsade de pointes". (a) Normal ECG indicating the P wave, QRS complex and T wave, as well as intervals typically measured. The T wave represents repolarization of the ventricle that is due to the outward movement K^+ ions across the cell membrane. In (b), a reduction in the outward K^+ current delays repolarization and prolongs the QT interval. The prolonged QT interval can lead to an abnormally rapid ECG or tachycardia (VT) that is characterized by a gradual change in the amplitude and twisting of the QRS complexes around the isoelectric line referred to as "torsade de pointes. Adapted from figure by Anthony Atkielski (CC BY-SA 4.0).

In patients, cardiac electrical rhythms are recorded with an electrocardiogram (ECG), which records the electrical potential changes of the heart over time, measured through electrodes placed on the skin (3,4). The appearance of a normal ECG is divided into distinct phases, as illustrated in Figure 1a. First, the atria depolarize (P wave) followed by a delay (PR interval) during which time the cardiac impulse propagates through the atrioventricular node (5). Thereafter there is a rapid depolarization of the ventricles (QRS complex) followed by the ST segment which reflects the plateau phase of the ventricular action potential. The repolarization of the ventricular action potential is reflected by the T wave and the QT interval represents the ventricular action potential duration.

At the cellular level, the action potential can be divided into five phases (3,6). By convention, a negative membrane potential means the inside of the cell is more negative than the outside, vice versa for a positive membrane potential. Normally an atrial or ventricular cardiomyocyte will have a stable resting membrane potential of about –85mV, which is referred to as Phase 4. This is due to a dominant potassium current referred to as the inward rectifier potassium current. When the cardiomyocyte is electrically stimulated sodium channels are activated resulting in the influx of Na^+ that generates the rapid upstroke phase of the action potential, referred to as Phase 0 (7). Upon depolarization a transient outward potassium current is activated which causes a partial and transient repolarization or notch, referred to as Phase 1 (7). The depolarization also activates both the L-type inward calcium current and delayed rectifier outward potassium currents which offset each other resulting in the plateau phase of the action potential, referred to as Phase 2 (7). This can last hundreds of milliseconds and corresponds to the time when the cardiomyocyte is in the refractory period and cannot be re-excited (6). With

time the calcium current diminishes, and the potassium currents become dominant so that there is a net outward current that is responsible for the repolarization phase, referred to as Phase 3. At the end of repolarization, the resting membrane potential is restored, and the cardiomyocyte recovers excitability (6).

2: hERG and Long QT syndrome

Differences from the standard ECG's can be indicative of heart disease, even in patients who exhibit few symptoms (8). A common abnormality is the Long QT syndrome (LQTS) which is caused by a prolongation of the QT interval that extends from the beginning of the QRS complex to the end of the T wave (Figure 1b). Typically, the QT interval is around 350 to 450 msec for adult men and from 360 to 460 msec for adult women. (9) The prolongation of the action potential can lead to abnormal transient depolarizations during phase 2, termed early afterdepolarization (EAD) that have been implicated in torsade de points. (9,10)

The *human ether-a-go-go related gene* (hERG), also known as *KCNH2*, encodes the $K_v11.1$ ion channel, also referred to as the hERG channel, that is responsible for the rapid delayed rectifier potassium current, I_{Kr} (11). I_{Kr} is a key generator of the potassium current during late portion of Phase 3 repolarization and has a major impact on the QT interval(11). hERG upregulation can cause the short QT syndrome (extremely rare) whereas hERG downregulation underlies the LQTS Type 2 (quite common). While up to 15 other ion channels have been implicated in LQTS the great majority of cases are attributed to mutations in hERG along with another delayed rectifier ion channel KCNQ1, the channel responsible for the slow delayed potassium current, I_{Ks} (12,13).

hERG dysfunction causing LQT2 can be either acquired or congenital (10). Acquired long QT syndrome typically occurs when drugs bind hERG as an off-target effect, or if there are imbalances in the ion concentrations(14). Congenital LQT2 is caused by point mutations in the gene that occurs at 1:2000 in Caucasian populations, with LQT2 making up 30-45% of LQT cases (12,15). A 2005 study identified 89 distinct hERG mutations in LQTS patients (16). Many of these have been studied in heteromeric systems, a summary of these mutations along with many others found in the literature are listed in Table 1. (16)

Those with congenital LQTS may not have significant symptoms before a major cardiac event occurs, hence it is a common cause of sudden death. However, genetic screening may be suggested if there is a family history of sudden death or a prolonged QT interval. The first line therapy for individuals with confirmed LQT2 are β--blockers (15). Sodium channel blockers, which have been shown to reduce the QT interval in patients with LQT2, have been proposed as a possible complementary therapy (17). If pharmaceutical treatments fail, an implantable defibrillator is considered, dependent on the risk profile of the individual (infections at implantation site and inappropriate shocks from defibrillator can have significant negative health consequences).

Table I: Summary of studied hERG mutants and their HI or DN phenotype. Adapted and updated from table by Tianci Wang (2020)

Mutant	Type	Domain	Phenotype	Experiments	Ref
R25W	Missense	N-term	DN	PC, WB	(18)
F29L	Missense	PAS	DN	automated PC	(19)
N33T	Missense	PAS	HI	automated PC	(19)
N33Y	Missense	PAS	HI	automated PC	(20)
I42N	Missense	PAS	DN	automated PC	(19)
N45D	Missense	PAS	HI	automated PC	(20)
N45H	Missense	PAS	HI	automated PC	(20)
G47C	Missense	PAS	HI	automated PC	(20)
L51V	Missense	PAS	HI	automated PC	(20)
Y54H	Missense	PAS	HI	automated PC	(20)
R56Q	Missense	PAS	?	automated PC	A19
C64R	Missense	PAS	HI	automated PC	(20)
L65P	Missense	PAS	DN	PC	(21)
L86R	Missense	PAS	DN	automated PC	(19)
V94M	Missense	Pas	HI	automated PC	(20)
Y99C	Missense	PAS	HI	automated PC	(20)
K101N	Missense	PAS	HI	automated PC	(20)
D102A	Missense	PAS	HI	automated PC	(20)
G103W	Missense	PAS	HI	automated PC	(20)
M124R	Missense	PAS	?	automated PC	(19)
W410R	Missense	VSD	DN	WB, PC, IF	(22)
L413P	Missense	VSD	HI	PC	(23)
T421M	Missense	VSD	?	PC	(24)
A422T	Missense	VSD	DN	automated PC	A19
D456Y	Missense	VSD	HI	PC	(25)
F463L	Missense	VSD	HI	PC, WB	(26)

N470D	Missense	VSD	DN	WB, co-IP	(27)
T473P	Missense	VSD	DN	PC	(28)
N474I	Missense	VSD	DN	PC	(29)
G487R	Missense	VSD	Mild	PC, WB	(30)
A558P	Missense	Pore	DN	PC, WB	(31)
L559H	Missense	Pore	HI	PC	(23,32)
A561V	Missense	Pore	DN	PC	(33)
A561T	Missense	Pore	DN	automated PC	(19)
A561V	Missense	Pore	DN	automated PC	(19)
I571L	Missense	Pore	HI	WB	(25)
I571L	Missense	Pore	DN	automated PC	(19)
G572S	Missense	Pore	DN	PC, c-ip, WB	(34)
G584S	Missense	Pore	DN	PC	(34)
I593R	Missense	Pore	DN	PC	(35)
G601S	Missense	Pore	DN	PC	(25)
G604S	Missense	Pore	DN	PC, WB	(36)
D609N	Missense	Pore	DN	automated PC	(19)
T613M	Missense	Pore	DN	automated PC	(19)
A614V	Missense	Pore	DN	PC	(29) (19)
E614V	Missense	Pore	DN	automated PC	(19)
L615F	Missense	Pore	DN	automated PC	(19)
T618S	Missense	Pore	?	automated PC	(19)
G628M	Missense	Pore	DN	PC	(33)
N629I	Missense	Pore	DN	automated PC	(19)
N629S	Missense	Pore	DN	automated PC	(19)
V630L	Missense	Pore	DN	PC	(29)
N633S	Missense	Pore	DN	automated PC	(19)
E637K	Missense	Pore	DN	PC	(37)

K638E	Missense	Pore	DN	automated PC	(19)
Q725X	Nonsense	CNBHD	HI	PC, co-IP, SGCA	(38)
R744P	Missense	CNBHD	Mild	PC, WB	(39)
R752W	Missense	CNBHD	DN	automated PC	(19)
F805C	Missense	CNBHD	HI	PC	(25)
G816V	Missense	CNBHD	HI	PC, WB, co-IP	(39)
S818L	Missense	CNBHD	DN	automated PC	(19)
V822M	Missense	CNBHD	DN	automated PC	(19)
R823W	Missense	CNBHD	DN	automated PC	(19)
N861X	Nonsense	CNBHD	DN	PC, co-IP	(40)
K897T	Missense	C-tail	?	automated PC	(19)
G903R	Missense	C-tail	?	automated PC	(19)
G965X	Nonsense	C-tail	DN	PC, co-IP	(41)
R1014X	Nonsense	C-tail	DN	PC, co-IP, SGCA	(41)
P1075L	Missense	C-tail	?	automated PC	(19)
P1085FX+32X	Frameshift	C-tail	?	PC, co-IP, WB	(38)
c3331-316G>T	Frameshift	Intronic	HI?	PC, WB	(42)

3: Structure and function of hERG

3a Structural domains

hERG specifically is the α-subunit of the ion channel, with KCNE2 (MiRP) being a regulatory β-subunit whose function is not well characterized (43). The hERG transcript is alternatively spliced into two isoforms: hERG 1a and hERG 1b, with 1b missing a large portion of the N-terminus region (44). However, 1b is not well characterized.

In 2017, the structure of hERG was obtained by cryo-electron microscopy (cryo-EM), significantly enhancing the understanding of hERG's structure-function relationship (45). Prior to

this, most of the structural information available on hERG was from homology models made with other related channels. The cryo-EM structure shows hERG in the open state, and is complemented by a structure of related channel EAG1 in the closed state (45).

The full length hERG protein (hERG-1a) is 1,159 amino acids long and consists of an N-terminal Per-Arnt-Sim (PAS) domain, a linker, 6 transmembrane α-helices S1-S6, and a C-terminal cyclic nucleotide binding homology domain (CNBHD) (11,45). Both the PAS and CNBHD face the cytoplasmic side. hERG 1b is 819 amino acids long and has a different N-terminal region, lacking the PAS domain (11). Instead, it has an ER-retention signal in its N-terminal region, leading to ER-retention unless the signal is covered by the N-terminal linker of hERG-1a (46). Hence hERG-1b does not traffic efficiently without the presence of hERG-1a (47). The subsequent domains are identical to hERG-1a (11,47).

The S1-S6 α-helices form the main structure of the channel, with the S1 to S4 helices comprising the voltage sensor and the S5-S6 helices forming the pore (11). Ion channel voltage sensors involve positively charged lysine and arginine residues on the S4 α-helix that for hERG includes K525, R528, R531, R534, R537, R538. When the membrane depolarizes, the S4 helix shifts upward to open the pore, and when it repolarizes, it shifts downward to close the pore (48). The S1-S3 helices have negative charges to counterbalance the positive ones on S4 (48), which occurs within the same subunit of the channel, so is referred to as *non-domain swapped*. This is in contrast to other potassium channels, for which the pore and voltage sensors from different subunits interact with each other(49,50).

The potassium selectivity filter of hERG resides in the outer pore domain where water molecules around hydrated K^+ ions in the pore are replaced by the carbonyl groups of amino acid residues 623 to 631, which comprise the selectivity filter. The selectivity filter of hERG is unique among the Kv family of channels by having Ser and Phe replace Thr and Tyr in the normal sequence Thr-Val-Gly-Tyr-Gly. The unusual position of Phe 627 confers hERG the unique property of fast C-type inactivation (51). The recent Cryo-EM structure has revealed four binding pockets in the hERG pore region just inside the selectivity filter that is unique among K^+ channels and is considered a likely cause of hERG's high promiscuity for drug binding (41). As a result, hERG screening is required for FDA approval of drugs, and this interaction has caused many drugs to have their use limited or to be withdrawn from use. Notably, the antihistamine terfenadine was withdrawn in 1997 due to its hERG-binding (52,53). In 2021, a first Cryo-EM structure of hERG bound to a drug, the antihistamine astemizole, was obtained (54). Astemizole (and likely other positively charged drugs) binds to a negative electrostatic potential created by nine aromatic (most notable Y652 and F656) and polar residues in this region, while hydrophobic drugs bind to four hydrophobic pouches mentioned above (54,55). In doing so, astemizole blocks K^+ flux through the channel by occluding the pore and preventing removal of the K^+ hydration sphere at the selectivity filter (54).

Other compounds exist which are purported to correct hERG trafficking, thus present a potential treatment method for LQT2. An issue with many such drugs which stabilize the protein during trafficking is that they bind and block the central pore of the channel(56). A notable example is E-4031. Recently, more promising candidates such as anagrelide and DCEBIO have been studied in our lab, although their efficacy has yet to be fully confirmed (57).

a

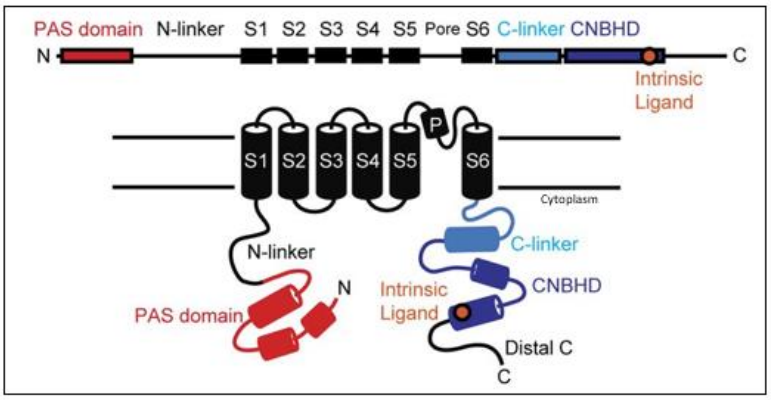

b

Domain	Amino acid range (approx.)
PAS	1-300
N-linker	300-400
S1-S5	400-600
Pore*	600-630
S6	630-660
C-linker	660-700
CNBHD	700-1150

c

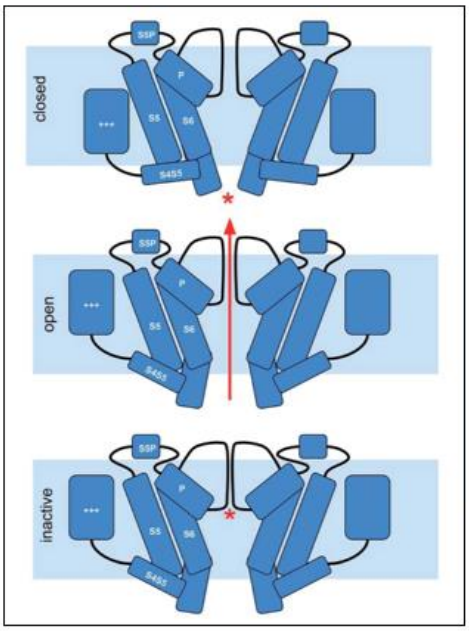

d

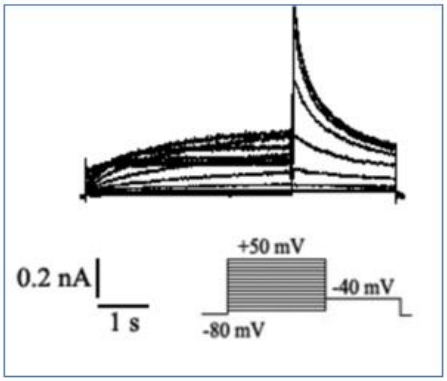

Figure 2: hERG domain structure and function. (a) Schematic diagram of the domains on a linear hERG polypeptide (top) and a in a folded subunit (bottom). This panel only shows one subunit for clarity, but hERG assembles as a tetramer. Adapted from Codding et al. (2019) (58). (b) List of domains and their amino acid ranges, * next to pore indicates that the range is only rough as the pore has a specific "pore helix" in the indicated range, but the S5 and S6 helices also form parts of the pore itself. (c) hERG cycles through three states. At resting potential, it is closed (meaning the ions cannot pass through the selectivity filter). Upon depolarization, K^+ ions may pass through the pore. hERG then rapidly inactivates, blocking the pore once again. After membrane potential begins to decrease, it returns to the open state. It then slowly closes again as the membrane repolarizes. Adapted from Kratz et al. (2017) with permission from the Royal Society of Chemistry. (59) (d) hERG current when assessed by the voltage clamp technique. Membrane is depolarized to various steps shown in bottom right, then repolarized to -40 mV. Measured current is traced over above with the scale shown at the bottom left. Excerpt from Long et al. (2013) (60).

The two intracellular domains, the PAS and CNBHD are involved in hERG's slow deactivation. Disease-causing mutants in the PAS domain have been shown to disrupt this interaction and speed up the channel's deactivation (61) PAS domains are highly structurally conserved, although their sequences are variable. They consist of 5 β-sheet strands along with alpha helices (62). The β-sheets respond to signalling and transmit the signal along the α-helices to the rest of the protein (62). In hERG, the PAS domain contains four α-helices (45). Its primary role is to interact with the CNBHD, permitting slow deactivation (61). Disease-causing mutants in the PAS domain have been shown to disrupt this interaction and speed up the channel's deactivation (61). The CNBHD is at the C-terminus of hERG and gets its name from homologous domains in other channels which bind to and are activated by cyclic nucleotides, such as cAMP (63). hERG's CNBHD shares a similar structure but has an intrinsic ligand: part of the domain itself binds and activates rather than a cyclic nucleotide (58). Specifically, F860, N861 and L862 (FNL motif) form the intrinsic ligand, and they interact with I804, G806, and N819 (58). The intrinsic ligand is required for the CNBHD to bind the PAS domain, which allows for the slow deactivation of hERG gating (to be described later) (49). The PAS and CNBHD interact in a domain-swapped manner: that is, the PAS from one subunit interacts with the CNBHD from the adjacent one (58).

Since hERG-1b lacks the PAS domain, the impact this has on hERG structure is unclear. However, heteromeric channels are found predominantly *in vivo*, and hERG-1b is shown to preferentially interact with hERG-1a. The lack of PAS domain means heteromeric channels would have fewer PAS-CNBHD interactions, and this configuration of the heteromeric channels corresponds with their observed faster deactivation kinetics. Preliminary data has shown that the N-linker region (Figure 2) interacts with the unique N-terminal portion of hERG-1b.

The aforementioned cryo-EM structure has provided many important insights to the structural components of hERG but is limited with respect to understanding functional dynamics by being "snapshots" of the protein. As such, other electrophysiological techniques are used to assess these aspects, and are discussed in the next section.

3b Electrophysiology of hERG, mechanism of inactivation/deactivation

The hERG channel exists in three states: closed, open and inactivated (6) (64). The transition from closed to open is referred to as activation and the return to the closed state is referred to as deactivation. On the other hand, the transition from open to inactivated is referred to as inactivation whereas the return to the open state is termed removal of inactivation. The conformation of hERG channels and corresponding I_{Kr} (rapidly inactivating delayed rectifier current) are voltage dependent (62, 63). At the negative resting potential of cardiomyocytes hERG channels are in the closed state and there is no I_{Kr}. Membrane depolarization slowly activates hERG channels, but before an appreciable I_{Kr} can be generated the channels undergo extremely rapid unique C-type inactivation at the selectivity filter (62, 63). This especially occurs at more positive potentials corresponding to the plateau phase of the cardiac action potential. This inactivation underlies the inward rectification of I_{Kr} and results in its minimal contribution during the plateau phase. Repolarization, which reverses the transitions in hERG seen during depolarization, causes rapid removal of hERG channel inactivation and channel opening. This underlies the increase in I_{Kr} that contributes to the latter phase of action potential repolarization. As the membrane approaches the resting potential the open hERG channels undergo deactivation that closes the channel and diminishes I_{Kr}. This occurs when the voltage sensor shifts with kinetics that are regulated by the interaction between the PAS and CNBHD (notably R56 and

D803) (64,65). The voltage dependent gating properties and kinetics of the hERG channel and I_{Kr} has been studied extensively principally using the whole-cell patch clamp technique and an array of different voltage step protocols described in detail in Vandenberg et al (2012) (6).

Small-molecule binding can also promote hERG activation and inactivation. The molecule PD-118057 appears to promote channel activation and counteract the effect of terfenadine (65). One hypothesis as to the mechanism is that it causes conformational changes in the S6 helix at residues Y652 and F656, which prevent terfenadine binding and attenuates inactivation (66).

4: Trafficking of hERG

As with all proteins, the KCNH2 gene is transcribed in the nucleus, producing three alternatively spliced isoforms. 1a, 1b and 3.1. The former two have previously been discussed. KCNH2-3.1 is expressed in the brain and is implicated in schizophrenia, but little is known about its function (67). The nascent transcripts eventually move to the rough endoplasmic reticulum (ER) for translation. Then, hERG moves to the Golgi apparatus before eventually moving to the cell surface.

In the ER, the immature hERG receives N-linked core glycosylation (CG) on the NX[S/T] motifs at N598 and N629 in the S5-S6 linked region. In the Golgi, mature hERG receives additional glycosylation and is termed fully glycosylated (FG). The differing molecular weights of these glycosylation patterns allow mature and immature hERG to have distinct bands on western blot.

a

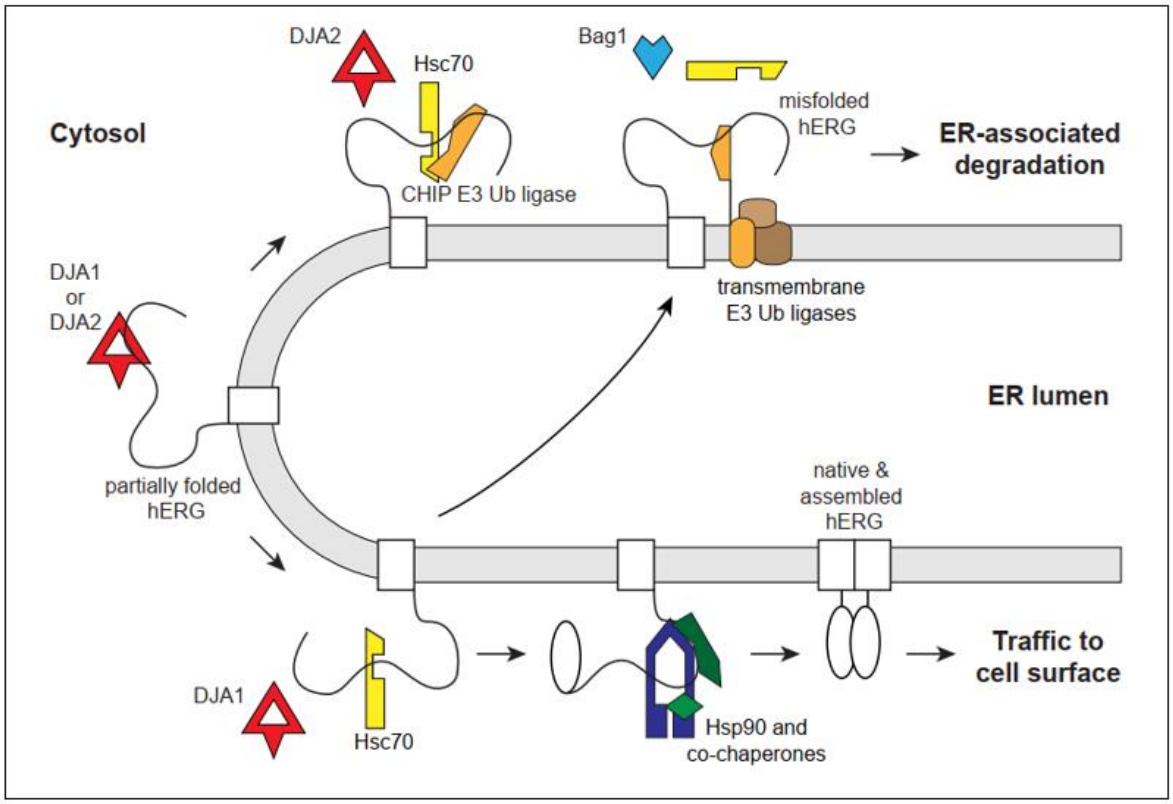
DJA2
Hsc70
Bag1
misfolded
hERG
Cytosol
ER-associated
degradation
CHIP E3 Ub ligase
DJA1
or
DJA2
transmembrane
E3 Ub ligases
ER lumen
partially folded
hERG
native &
assembled
hERG
Traffic to
cell surface
DJA1
Hsc70
Hsp90 and
co-chaperones

b

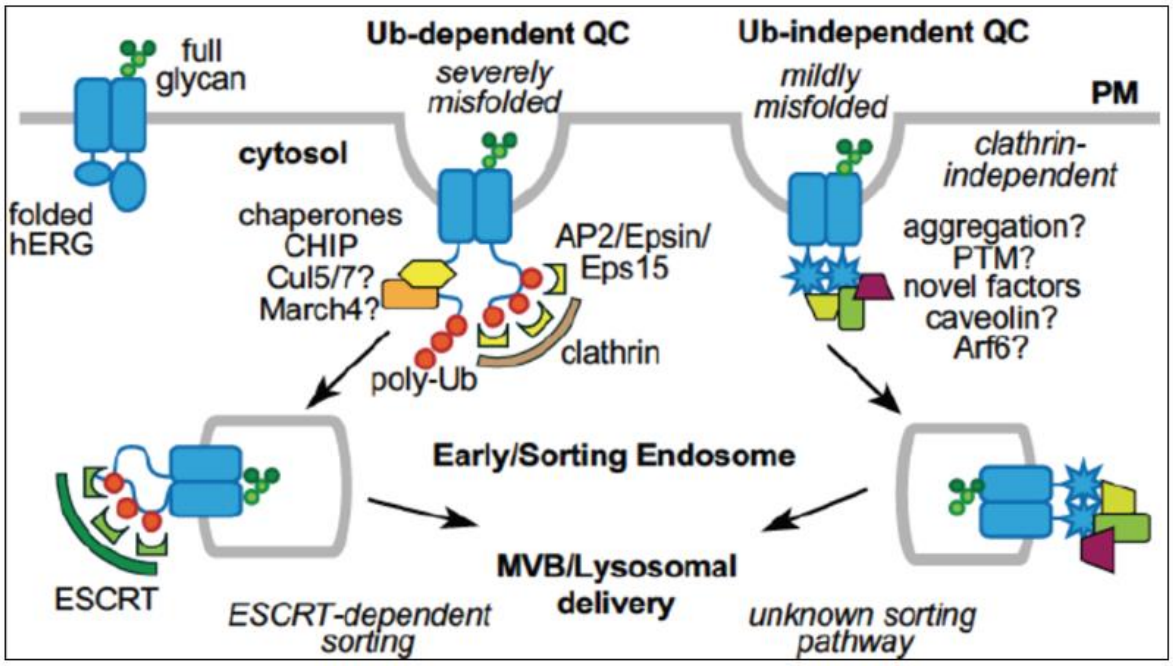
full
glycan
Ub-dependent QC
severely
misfolded
Ub-independent QC
mildly
misfolded
PM
cytosol
clathrin-
independent
folded
hERG
chaperones
CHIP
Cul5/7?
March4?
AP2/Epsin/
Eps15
aggregation?
PTM?
novel factors
caveolin?
Arf6?
clathrin
poly-Ub
Early/Sorting Endosome
ESCRT
MVB/Lysosomal
delivery
ESCRT-dependent
sorting
unknown sorting
pathway

Figure 3: Protein quality control in hERG trafficking and folding (figures drawn by Jason Young). (a) hERG subunits are assembled and folded in the ER. Hsc70 and its co-chaperones DJA1 and DJA2 are crucial to the folding process. If hERG does not fold correctly, the E3 ligase CHIP is recruited and polyubiquitinates hERG, leading to proteasomal degradation. Hsp90 competes with CHIP for binding to hERG (mediated by HOP) and continues the maturation process. (b) hERG can misfold on the plasma membrane as well, and depending on the severity of the misfolding, it is endocytosed either by a ubiquitin-dependent mechanism (left) mediated in clathrin-coated vesicles or by a ubiquitin independent (right) mechanism. The misfolded protein is then sorted and degraded in the lysosomes.

Due to mutations, environmental or physiological stressors, hERG protein may not be able to fold to its native conformation. Improperly folded proteins can have deleterious effects on the cell. As a result, quality control (QC) mechanisms exist to help hERG fold. The main control point in hERG trafficking is in the ER (ERQC), with chaperones aiding in folding, and ER-associated proteasomal degradation (ERAD) occurring in the case where proteins cannot be folded (68).

The main chaperones involved in hERG folding in the ER are the ATP-dependent Hsp70 and Hsp90, along with several co-chaperones which interact with Hsp70 and Hsp90. The Hsp70 ATPase cycle requires activating proteins (DNAJ family) and nucleotide exchange factors (69). In hERG folding, DNAJA1, A2, B12 and B14 have been identified, with these DNAJB's being of particular importance for tetramerization because of their transmembrane domains (Figure 3a) (70). The nuclear exchange factors (NEFs) precisely involved with hERG are not well known, however BAG1 has been shown to interact with hERG, promoting its degradation by mediating an interaction with E3-ubiquitin ligase CHIP. Other E3 ligases such as rififylin ubiquitinate hERG, but their regulation is not well understood (71). Hsp90's hERG-binding is mediated by HOP, which competes with CHIP due to their shared TPR-domain (72). As such, one manner by which Hsp90 promotes hERG folding is by blocking its ubiquitination (68). Polyubiquitinated hERG is subsequently degraded by the proteasome.

If hERG makes it to the plasma membrane, but starts to misfold once there, it can be dealt with by one of two mechanisms, illustrated in Figure 3b. If the hERG on the plasma membrane becomes severely misfolded it is recognized by the Hsp70 system, ubiquitinated by CHIP and internalized in clathrin-coated vesicles (71). The vesicles are then delivered by ESCRT proteins to the lysosome and degraded (71). If hERG is mildly misfolded, as in the case of PAS domain

mutants, it is internalized by a ubiquitin and clathrin independent mechanism and targeted for lysosomal degradation (48).

Since LQT2 is autosomal dominant, patients have variations of the hERG gene expressed. One is the WT gene, the other is the mutant. The effect of the mutant depends on whether it interacts with the WT protein. If they do interact, it is reasonable to assume that the misfolding mutant, causes the tetrameric channel to misfold. This is called a dominant negative (DN) effect. If they do not interact, this means only the hERG translated from the WT mRNA is making it to the cell surface. Hence, one would expect approximately half the number of channels to be expressed as compared to patients without the disease. This condition is referred to as haploinsufficiency (HI). The DN and HI mechanisms are illustrated in Figure 4.

Most mutants appear to be dominant negative. Ng et al. found that roughly 90% of mutants in the PAS domain were DN, with HI mutants representing roughly 5% (20).

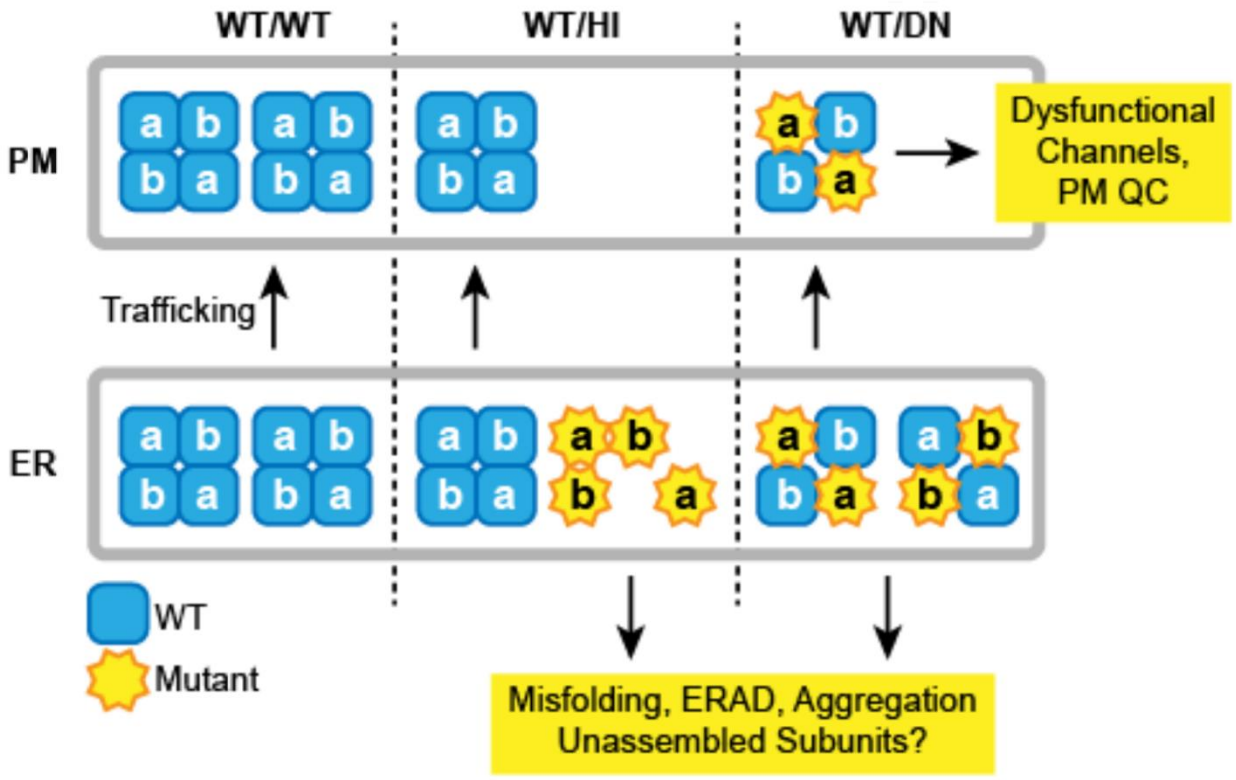

Figure 4: The haploinsufficient (HI) and dominant negative (DN) mechanisms of hERG trafficking (figure drawn by Jason Young). Four variants of hERG are translated from the mRNA. From each allele, hERG 1a and 1b are produced. If one allele is a mutant, there are two possibilities for the fate of the mutant protein. First, if the mutant is too severely misfolded to tetramerize it is degraded by the ER quality control systems. In this case, only the WT protein reaches the cell surface, but only at a half dose since it originates from a single allele. This is the HI mechanism. The second case is where the mutant can associate with the WT protein. The mutant may cause misfolding of the whole tetramer, and lead to degradation by either ER quality control or PM quality control. In either case, the mutant suppresses expression of the WT protein. This is the DN mechanism.

5: Channels related to hERG

hERG's trafficking is less well characterized than other similar channels. A more studied channel which frequently suffers from folding difficulties is CFTR, a chloride channel implicated in Cystic Fibrosis (CF)(73). Unlike hERG, CFTR is one large subunit with four pore domains. The most common delta-F508 mutation found in 82% of patients leads to misfolding, upon which it is recognized by the ER quality control machinery and subsequently degraded (74). Likewise, DJA1, DJA2, Hsc70 and CHIP act in concert for the plasma membrane quality control (74). When this occurs, CFTR is internalized by clathrin-mediated endocytosis and degraded in the lysosome (74).

Although older treatments for CF involve treatment of the symptoms, in recent years more targeted therapies have been developed, and much work is being done to find similar compounds for hERG. To date, four CFTR modulators have been approved for use: ivacaftor, lumacaftor, tezacaftor and elexacaftor (they are used in combination therapies) (75). For delta-F508, two types of drugs have been shown to correct folding (75). First, pharmacological chaperones directly bind misfolding CFTR, and help it pass QC checkpoints (75). Second are proteostasis regulators, which target the checkpoints that prevent mutant CFTR trafficking. However, since these target chaperones instead, the chances of off-target effects are greater (75).

Compounds that correct hERG mutations pose a greater challenge because there is no single mutant presnet in most patients. Hence, the likelihood that a single compound will aid a large population of LQT2 patients is low.

Due to their similarities, the studies done on CFTR are a major source of the paradigm for hERG trafficking and folding (2). However, it is worth noting that hERG and CFTR appear to exhibit some differences with the specific co-chaperones involved in the quality control steps, as there is specificity in the QC pathways.

6: Transfection, a method for expressing genes outside their normal context

To study proteins such as hERG, it is not always practical to study them in their native environment. There is a hierarchy of potential methods that can be used that involve near-native primary cells taken from patients (complicated and expensive to obtain) to studying purified proteins in a tube (easy to use but with uncertain relevance to the native system).

Cultured cell lines typically represent a good middle ground. They have all the features required for a cell to survive and can be grown continuously in a dish. Of course, the factors that allow them to grow well in a dish mean they differ significantly from an *in vivo* system. Even within the range of cell lines, there exist a range of choices. For studying hERG, the most physiologically accurate cell line would be a cardiomyocyte line such as HL-1 cells or cardiomyocytes made from pluripotent stem cells (76).

Other cell lines, usually the easiest to use in assays, are farther from the native environment and do not necessarily express the protein of interest. In the case of this study, HeLa and HEK-293 cell lines are used. Hence, the protein of interest, hERG in our case, needs to be introduced.

Introducing non-native nucleic acids to a cell is called *transfection*, and it can be done in many ways. First, there is the distinction between *transient* and *stable* transfections. A *transient*

transfection, as the name implies, is one in which the exogenous nucleic acid remains temporarily in the cells (77). A *stable* transfection permanently inserts the DNA sequence to the cells' genomes (77). Transient transfections are useful for their flexibility and typically do not take long to prepare. In comparison, stable transfections are more laborious to prepare, but are useful if the gene of interest must be expressed in a consistent manner.

Transfection can be achieved using engineered viruses or by physical methods such as electroporation. The simplest method to use, however, is chemical transfection. Chemical reagents are commercially available, which can be mixed with the DNA and put on the cells. They consist of lipid-like molecules with polar and non-polar moieties (78). No special equipment is required, and they are less hazardous than viral methods. They form complexes with the DNA and fuse with the cells (78). There are trade-offs for the flexibility and ease-of-use of this technique largely due to the stochastic nature of these interactions (77). The transfection efficiency and hence overall expression are lower. Furthermore, the expression per cell is highly variable, which poses a challenge if quantitative microscopy studies need to be done (79).

Transient transfections typically cause protein to be produced at levels significantly higher (per cell, observed signal may still be low if few cells get transfected) than they would natively due to high amounts of DNA per cell and the use of viral promoters such as cytomegalovirus (CMV) (80). When dealing with large multimeric transmembrane proteins like hERG, translation and folding of the resultant polypeptides may overload the ER and reduce expression of each component during co-transfection (81).

Stable transfections require more elaborate methods, as the DNA must enter the genome. Hence, chemical methods on their own do not suffice. Traditional methods use lentiviral infection, however these integrate the gene of interest randomly into the genome and may integrate multiple times. Newer methods such as targeting the DNA with CRISPR-Cas9 or using specially engineered cell lines can make cell lines more comparable (77). In this project, we will be using engineered Flp-In cell lines, which are described in greater detail in the **Methods** section.

Objectives and Hypotheses

Previous studies have characterized over 30 disease-causing mutants, with about 30 more recently characterized by automated patch clamping (19). However, these studies worked with hERG-1a heteromers, which less closely resemble native currents than 1a/1b heteromers (82). Patch clamping studies are limited: they only tell us to what extent normal current is impaired or modified, but not *how* these effects occur. As such, we aimed to examine mutant hERG interactions in greater depth. To do so, we created a co-expression system in HEK-293 Flp-In TREx cells, allowing for the inducible co-expression of both 1a and 1b hERG. Combinations with WT and mutant 1a and 1b were made.

Due to a variety of technical and logistical challenges, this thesis primarily sets up an expression system where further mutants can be explored, demonstrating its effectiveness with a few mutants. We chose two severe mutants, G601S and F805C, which exhibited contrasting expression profiles in previous work done in our lab by Tianci Wang. Namely, we hypothesize G601S to be DN and F805C HI. Furthermore, mutations in hERG-1a should have dominant negative effects regardless of the mutant, when co-expressed with WT hERG-1b. This is a result of previous literature showing that hERG-1b cannot traffic on its own (47).

Results

To facilitate detection of hERG, hemagglutinin (HA) and myc epitope tags were inserted into its DNA sequence. The epitope tags serve two functions. First, to differentiate between different versions of hERG (mutants and isoforms) co-expressed in the experiments. Second, to allow for detection of hERG at the cell surface the tags were inserted in an extracellular loop between the S1 and S2 helices. Each tag was added to both 1a and 1b hERG isoforms. Hence, four WT constructs were produced, referred to as 1a-HA, 1a-myc, 1b-HA and 1b-myc. For later experiments, 1a-HA and 1b-myc were used exclusively.

Mature cell-surface hERG can be identified by proxy using molecular weight due to changes in glycosylation: immature hERG 1a and 1b give bands at 135 and 90 kDa, respectively (47). Mature 1a and 1b give bands at 155 and 110 kDa, respectively (47).

1: Transient transfections are not suitably reproducible for hERG co-expression experiments

Following positive results in pilot experiments by a previous student in our lab, we initially considered transient transfections as the optimal experimental protocol to observe hERG expression. As hERG maturation (i.e. hERG FG expression levels compared to CG) was observed to be significantly higher in HeLa cells versus HEK-293 cells, HeLa cells were used for these experiments.

Given that we had produced the four WT constructs, mutants could be generated by site-directed mutagenesis. Accordingly, several such mutant constructs were prepared by the previous student but not used in this study. This protocol allowed for the inclusion of null-allele controls, particularly of use to observe the HI mechanism. It was desired that the expression of WT HA-tagged hERG alone be equal to that of WT HA-tagged hERG when co-expressed with WT

myc-tagged hERG (and correspondingly with HA and myc swapped, which will be omitted for brevity).

For this null-allele control, we observed that hERG-HA expressed at greater levels with empty vector than with hERG myc. A possible explanation for this lies with the mechanism behind transient transfections described in section 6 of the introduction. In short, hERG may overload the ER and reduce expression of each component during co-transfection, hence more is able to be expressed in single transfection. Using an unrelated ion channel, KCNQ4 (HA and myc tagged, abbreviated as "Q4"), to equalize the transfected DNA amount led to more comparable expression levels. This channel was chosen due to its differing size from hERG and the lack of literature showing any interaction between the two.

Initially, we attempted to optimize transfections to minimize noise. Different reagents, amounts of DNA and amounts of cells were attempted and are shown in Figure 5a. Fugene 6 was the starting reagent, used previously by our lab. Other chemical transfection reagents were attempted. Data from ProMega indicated that transfection efficiency of Fugene HD was higher in HeLa cells, and Lipofectamine 2000 was also readily available. Lipofectamine decreased cell viability, so immunoblots could not be performed on these samples. No significant improvement in variability or expression levels was seen with Fugene HD, hence Fugene 6 was maintained for other experiments.

a

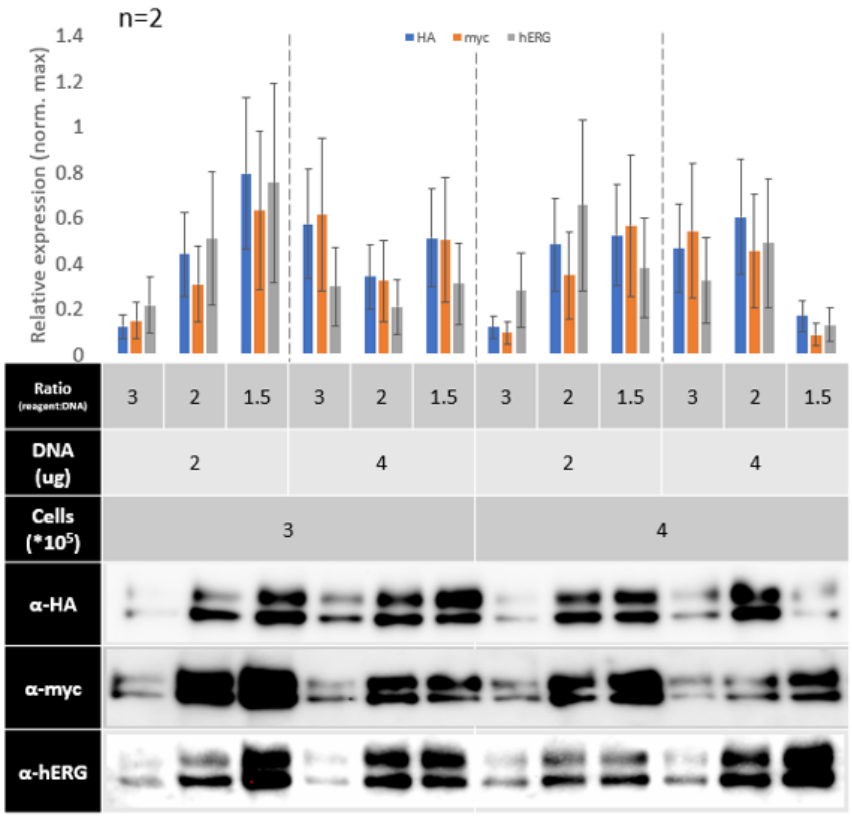
n=2
HA
myc
hERG
Relative expression (norm. max)
1.4
1.2
1
0.8
0.6
0.4
0.2
0
Ratio (reagent:DNA)
3 2 1.5 3 2 1.5 3 2 1.5 3 2 1.5
DNA (ug)
2 4 2 4
Cells (*10^5)
3 4
α-HA
α-myc
α-hERG

b

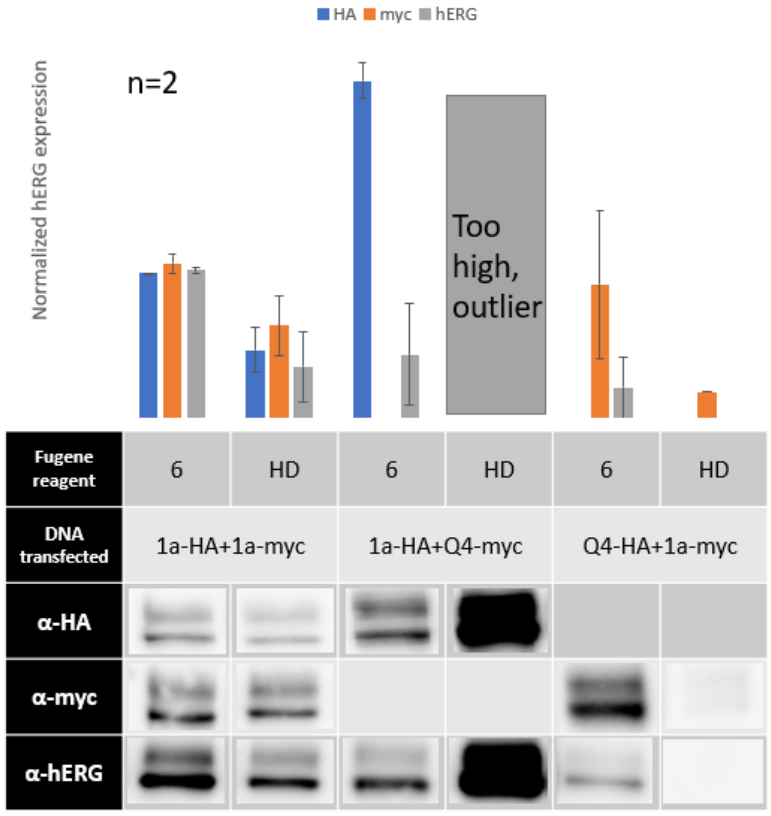
HA
myc
hERG
n=2
Normalized hERG expression
Too high, outlier
Fugene reagent
6 HD 6 HD 6 HD
DNA transfected
1a-HA+1a-myc
1a-HA+Q4-myc
Q4-HA+1a-myc
α-HA
α-myc
α-hERG

Figure 5: Transfection reagents and ratios do not affect transiently transfected hERG variability.

(a) Different amounts of DNA and transfection reagent-to-DNA ratios were used to assess the variability and strength of hERG expression. For each blot, the maximum hERG-FG band was set to 1 and the remaining data points were plotted as a proportion of 1. Experiments were repeated twice, and error bars show the range. (b) Fugene 6, Fugene HD and Lipofectamine 2000 transfection reagents were tested to assess the variability and strength of hERG-FG expression. 1a-HA/1a-myc co-expression as well as expression with KCNQ4 (Q4) HA or myc were tested. Lipofectamine killed cells, thus could not be blotted for. For each blot, the maximum hERG-FG band was set to 1 and the remaining data points were plotted as a proportion of 1 (excluding outlier condition indicated, roughly 3X the second highest). Experiment was repeated twice, and error bars show range.

As an alternative attempt to improve expression levels and reproducibility, the transfection reagent to DNA ratio was changed. Chemical transfection reagents such as Fugene 6 consist of lipid-like molecules with polar and non-polar moieties. They form complexes with the DNA and fuse with the cells. These complexes need to be optimally charged (neutral-to-slightly positive) and amount of reagent/DNA required for this depends on the specific conditions of the experiment. If efficiency is low, this means few cells are expressing the protein. As a starting point, we used a 3:1 reagent-to-DNA ratio with 2 ug total DNA. From there, we tried reducing the amount of reagent. The results of this experiment are shown in Figure 5b. Because the 1.5:1 reagent:DNA ratio with 2 ug DNA showed qualitatively higher expression and used the least reagent and DNA, this condition was chosen for subsequent transient transfection experiments.

In brief, the experiments from Figure 5 show that a 1.5:1 Fugene 6 to ug DNA ratio with 2 ug DNA gave the highest expression level and most reproducible expression.

With 2 ug DNA at a reagent:DNA ratio of 2:1 chosen; five repetitions of these co-transfections were performed to determine the variability of expression. The expression levels of the FG form of hERG were quantified on HA, myc and hERG blots (both 1a and 1b bands) and normalized to the condition of wild-type co-expression (1a or 1b), which was set equal to one. Student's t-tests were conducted on the results for the mutants, comparing the expression to the wild-type co-expression condition. These results are shown in Figure 6. G601S and F805C mutants did reduce mature hERG expression to levels significantly below WT (Figure 6a, b). However, no statistically significant differences were found between mutants (Figure 6c). As shown by the data in Figure 6, this method was not considered sufficient for us to compare hERG mutants.

a

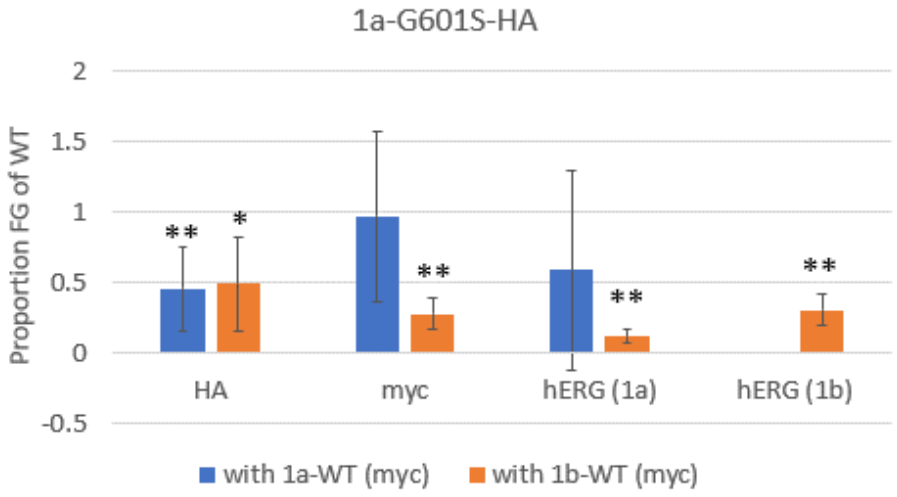
1a-G601S-HA
Proportion FG of WT
2
1.5
1
0.5
0
-0.5
**
*
**
**
**
HA
myc
hERG (1a)
hERG (1b)
with 1a-WT (myc)
with 1b-WT (myc)

b

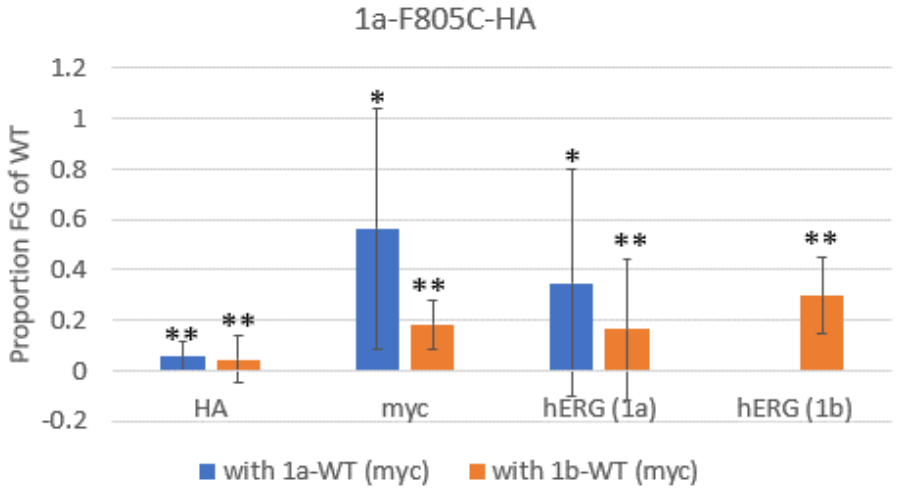
1a-F805C-HA
Proportion FG of WT
1.2
1
0.8
0.6
0.4
0.2
0
-0.2
**
**
*
**
*
**
**
HA
myc
hERG (1a)
hERG (1b)
with 1a-WT (myc)
with 1b-WT (myc)

c

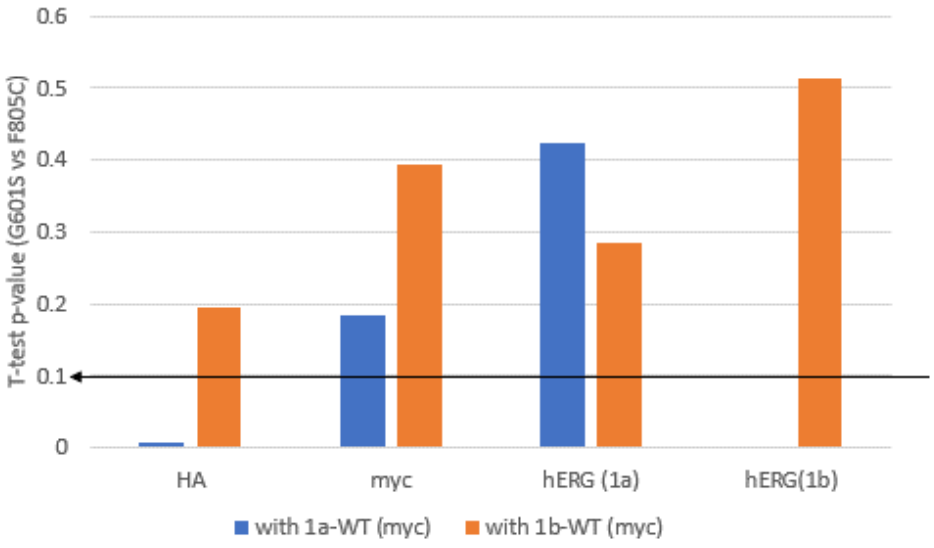
T-test p-value (G601S vs F805C)
0.6
0.5
0.4
0.3
0.2
0.1
0
HA
myc
hERG (1a)
hERG(1b)
with 1a-WT (myc)
with 1b-WT (myc)

Figure 6: Transient transfections are sufficient to detect differences between WT and mutant hERG expression, but not between two mutants. hERG 1a-myc WT or hERG 1b-myc WT was co-expressed with hERG 1a-HA in HeLa cells with the 1a unit being WT, G601S or F805C mutants. The level of mature hERG was expressed by observing the FG band on HA, myc and hERG western blots. Panels (a), (b), and (c) represent the results of n=5 experiments. (a) and (b) show the relative FG expression of the G601S and F805C mutants compared to the WT, respectively. Note that in the section representing the hERG (1a) blot, both WT and mutant would overlay to one band during 1a/1a co-expression. Error bars represent average percent error. (c) shows the p-values when comparing G601S and F805C, with 0.1 labelled as a cut-off for significance. * = $p<0.1$ ** = $p<0.05$

2: Stable cell lines expressing inducible hERG isoforms: a more reliable method to study mutants

Given that our objective was to compare the effects of different mutants to each other, the approach outlined in section 1 was not sufficient. Previous work published in our lab used stable cell lines for hERG expression, as it is less laborious (cells require little-to-no manipulation before assays) and more reproducible in the long term (not dependent on commercial products to express the protein). This is also closer to the native environment the protein is in: rather than *some* cells expressing hERG at a very high level, *all* cells will express hERG at a lower level. To this end, we used the HEK293 Flp-In TREx cell line, which allows for the integration of the target gene to the genome at a specific location where its expression can be induced with tetracycline/doxycycline via the Tet operon.

To use our differentially tagged hERG constructs in this system, we assembled bicistronic vectors containing hERG-1b with a myc tag and hERG-1a with a HA tag (see full description in **Methods**).

For most experiments in this section, only two cell lines were used. Cells co-expressing hERG WT 1b-myc and hERG WT 1a-HA (abbreviated WT/WT), as well as cells co-expressing hERG G601S 1b-myc and hERG WT 1a-HA (abbreviated G601S/WT). This was because of difficulty encountered in generating the clones. After more than a year of trying various strategies that were unsuccessful, it was decided to have the clones made commercially by a company with extensive expertise in cloning. Due to the challenge of cloning hERG this company also struggled and was unsuccessful. So, after many months a second company was approached. They also struggled but finally after upwards of a year they were able to generate the G601S/WT construct,

which was used as the representative mutant. The other constructs were delayed further and only began to arrive months later too late to be included in this thesis.

Overall immunoblot signal strength was compared between transients and stable cell lines (not shown), and the stable cell lines had several orders of magnitude more hERG expression. The Flp-In TREx system is titratable in theory, so we attempted different concentrations of doxycycline for induction of hERG expression and observed it by immunoblotting (not shown). The expression of the hERG constructs did not vary significantly from 1 ng/mL to 1 ug/mL doxycycline. Hence, 10 ng/mL was used for future assays.

The expression of the hERG constructs was assessed by immunoblot for WT/WT and G601S/WT as well as two additional constructs: WT/G601S and WT/F805C. The FG and CG expression normalized to WT/WT (set to 1) is shown in Figure 7. For the former two constructs, more repetitions were completed, but are shown separately in Figure 9 (as input). Looking at mature hERG (Figure 7a), there is a decrease in expression to roughly 80% of the WT when co-expressed with 1b-G601S. The expression of WT 1b when co-expressed with either mutant appears to increase by 20-30%. However, aside from lower mature expression of the F805C mutant itself, little difference is distinguishable between the two conditions.

Fitting with the decreased FG signal for F805C, this mutant has enriched expression of immature F805C (Figure 7b). In comparison, immature G601S remains consistent whether expressed as 1a or 1b. In brief, the data in Figure 7 demonstrates that both G601S and F805C reduce WT hERG expression, and F805C mutant hERG accumulates in its immature form, without significant effect on the mature form.

To observe the subcellular localization of hERG, the HEK-293 Flp-In TREx stable cells expressing WT/WT were transfected with mCherry tagged marker plasmids for the ER, Golgi, endosomes, lysosomes, and the plasma membrane. Aside from the CFTR plasmid, which was used for previous experiments, the remainder were gifts from Michael Davidson (see **Methods**). The resultant images are shown in Figure 8.

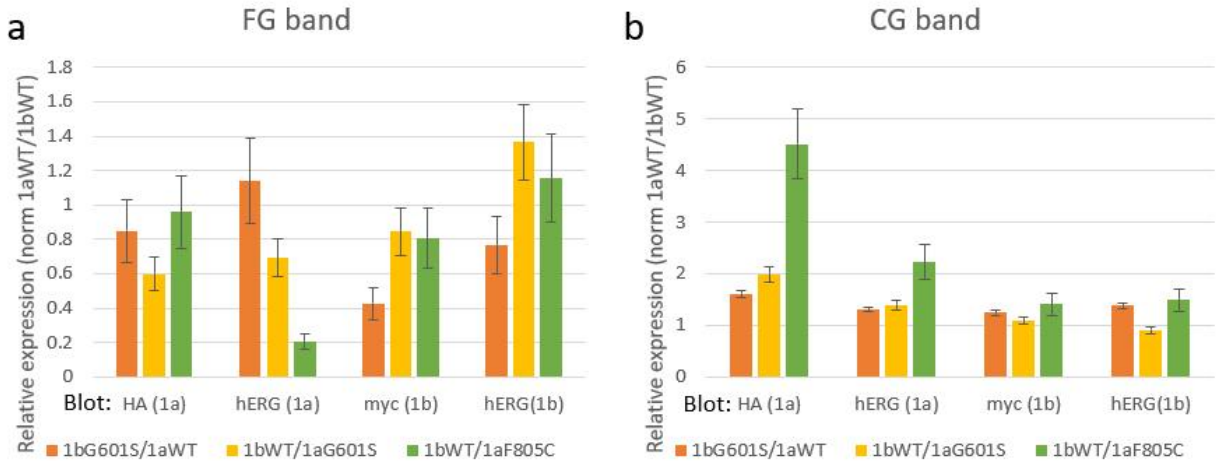
a
FG band
Relative expression (norm 1aWT/1bWT)
1.8
1.6
1.4
1.2
1
0.8
0.6
0.4
0.2
0
Blot: HA (1a)
hERG (1a)
myc (1b)
hERG(1b)
1bG601S/1aWT
1bWT/1aG601S
1bWT/1aF805C
b
CG band
Relative expression (norm 1aWT/1bWT)
6
5
4
3
2
1
0
Blot: HA (1a)
hERG (1a)
myc (1b)
hERG(1b)
1bG601S/1aWT
1bWT/1aG601S
1bWT/1aF805C

n=2

c

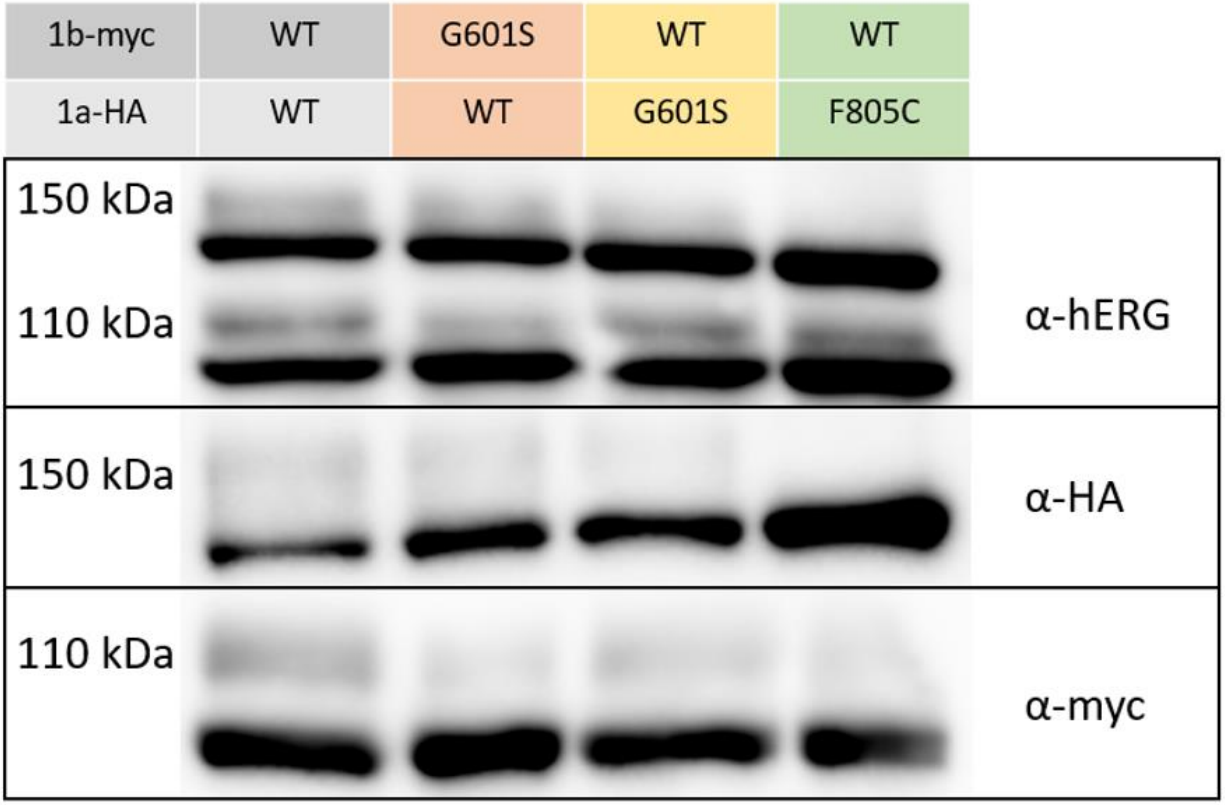
1b-myc
WT
G601S
WT
WT
1a-HA
WT
WT
G601S
F805C
150 kDa
110 kDa
α-hERG
150 kDa
α-HA
110 kDa
α-myc

Figure 7: hERG expression levels in stable HEK-293 FlpIn TREx cell lines. Cell lines were made stably expressing a bicistronic sequence with both hERG-1b-myc and hERG-1a-HA. Several combinations are shown here, as indicated in (c) with colours matching the charts in (a) and (b). (a) and (b) show the relative hERG expression for each condition compared to the WT/WT condition, which is set to 1. As this experiment was done n=2 times, error bars represent range. (c) shows an example blot along with a table of all the combinations used.

The signal for the plasma membrane (CFTR) transfections was very weak and should be repeated with a better marker protein. The wild-type hERG appears enriched in the Golgi when expressed with 1b-G601S, and greater co-localization is seen as compared with the WT. Similarly, co-localization appeared greater in conditions where the mutant was expressed for the ER marker.

Next, to look directly at the association of the hERG channels, co-immunoprecipitation experiments were performed. Magnetic beads conjugated with α-HA and α-myc antibodies were used to pull hERG down. Then blots for the opposite (α-myc blot if α-HA antibody was used) antibody reflected the level of associated protein pulled down. The results are summarized in Figure 9. Notably, in the co-immunoprecipitation condition we see an enrichment of the FG band (observed by FG/CG ratio) compared to the input. The enrichment of the FG band is more substantial for the W/W condition as compared to the G/W condition. This suggests that hERG-1b G601S does associate with hERG-1a WT, but not as strongly as hERG-1b WT. More repetitions would be required to attain statistical significance. However, this data shows preferred association between wild-type subunits.

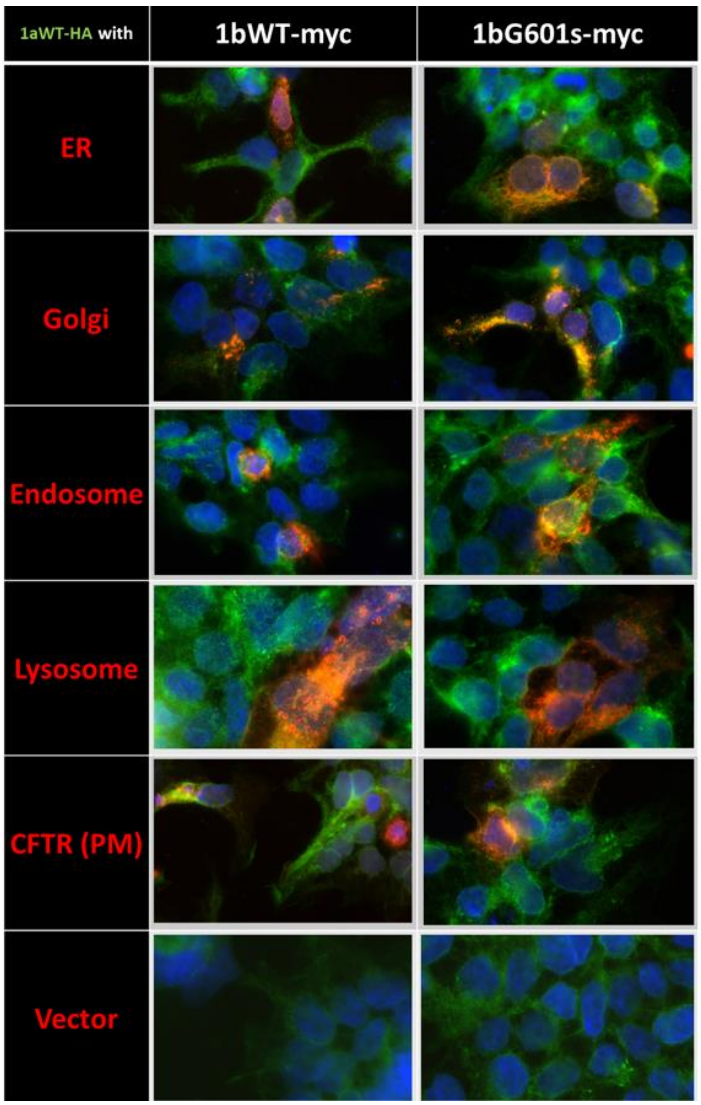
1aWT-HA with
1bWT-myc
1bG601s-myc
ER
Golgi
Endosome
Lysosome
CFTR (PM)
Vector

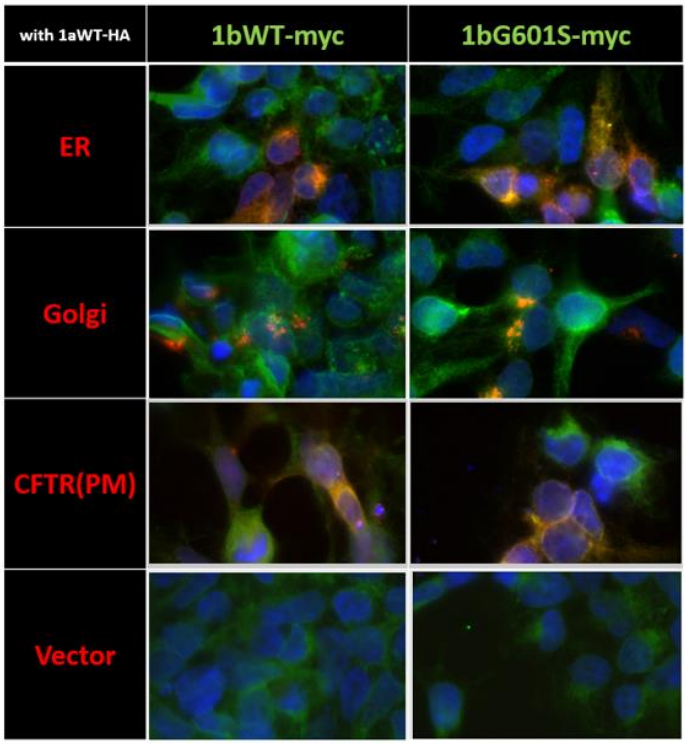
with 1aWT-HA
1bWT-myc
1bG601S-myc
ER
Golgi
CFTR(PM)
Vector

Figure 8: hERG WT and G601S intracellular localization compared with various markers. HEK 293 Flp-In TREx cells stably co-expressing hERG-1a-HA and either hERG-1b-myc or hERG-G601S-1b-myc were transfected with mCherry marker plasmids (indicated in red text) for intracellular compartments. The cells were then stained with antibodies for HA (left panel) or myc (right panel) and imaged on a confocal laser scanning microscope. Sample images are shown for each condition. On the left, α-HA primary antibodies were bound to green fluorescent secondary antibodies, rendering the 1aWT-HA signal green. On the right, α-myc primary antibodies were bound to green fluorescent secondary antibodies, rendering the 1bWT-myc or 1bG601S-myc signals green.

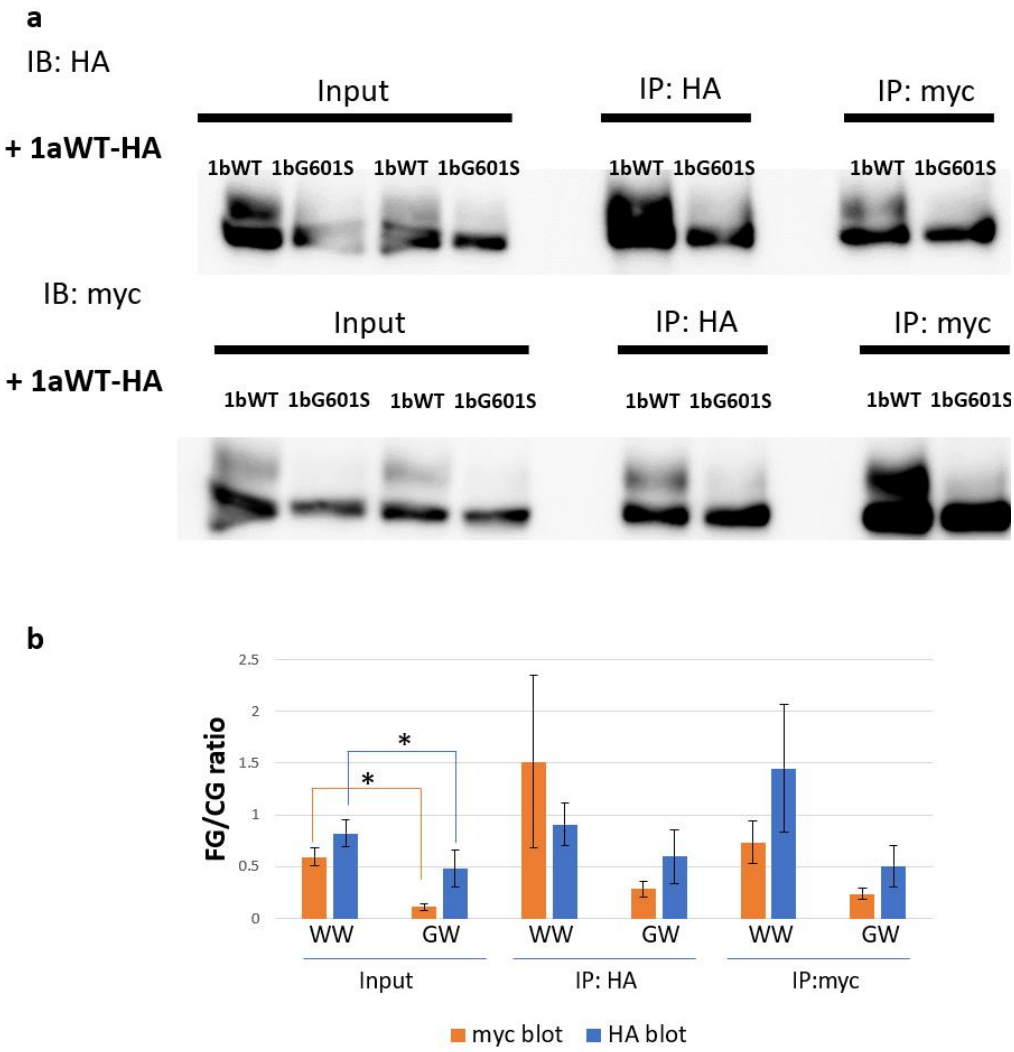

Figure 9: Co-immunoprecipitation of hERG 1a and 1b in HEK-293 FlpIn TREx cells. Cells stably expressing hERG-1b-myc WT/hERG-1a-HA WT (WW) and hERG-1b-myc G601S/hERG-1a-HA WT (GW) were lysed. HA (IP:HA) or myc (IP:myc) tagged proteins were pulled down from cell lysates. Eluates from the beads were immunoblotted: (a) Immunoblot images for one replicate of co-immunoprecipitation experiment. (b) Summary of data for all replicate immunoprecipitation experiments n=2-6, error bars indicate standard deviation (except IP's myc blot where n=2, and they indicate range). * = $p<0.001$

To assess how much hERG is directly on the cell surface (as opposed to mature hERG protein), the stable cell lines expressing WT/WT and G601S/WT were treated with Sulfo-NHS-SS-Biotinbiotin (sulfosuccinimidyl-20(biotinamido)ethyl-1,3-dithiopropionate), which binds to primary amines of proteins. Since the cells were not permeabilized, only proteins on the cell surface were labelled. Lysates were then prepared from these biotinylated cells and biotinylated protein was pulled down with streptavidin beads. hERG was probed by immunoblot for HA, myc and hERG. To determine whether the mutant was reaching the surface less efficiently than the WT/WT, the FG to CG ratio was determined. A higher FG:CG compared to input would indicate enrichment of mature hERG, as one would expect in this biotinylation experiment. The ratios in the input and biotinylated lysates were calculated and are shown in Figure 10a, along with the immunoblot images shown in Figure 10b. The signal for immature hERG was not non-existent in the biotinylated samples, however there was a strong enrichment for FG in biotinylated hERG. The enrichment is slightly higher for the G601S/WT mutant, however a much smaller proportion of the total hERG was pulled down for either mature or immature mutant, as compared to WT/WT.

Combined, the results in Figure 10 show that both a lower proportion of hERG-1b-G601S reaches the cell surface, and less hERG-1a-WT reaches the surface when co-expressed with the G601S mutant.

a

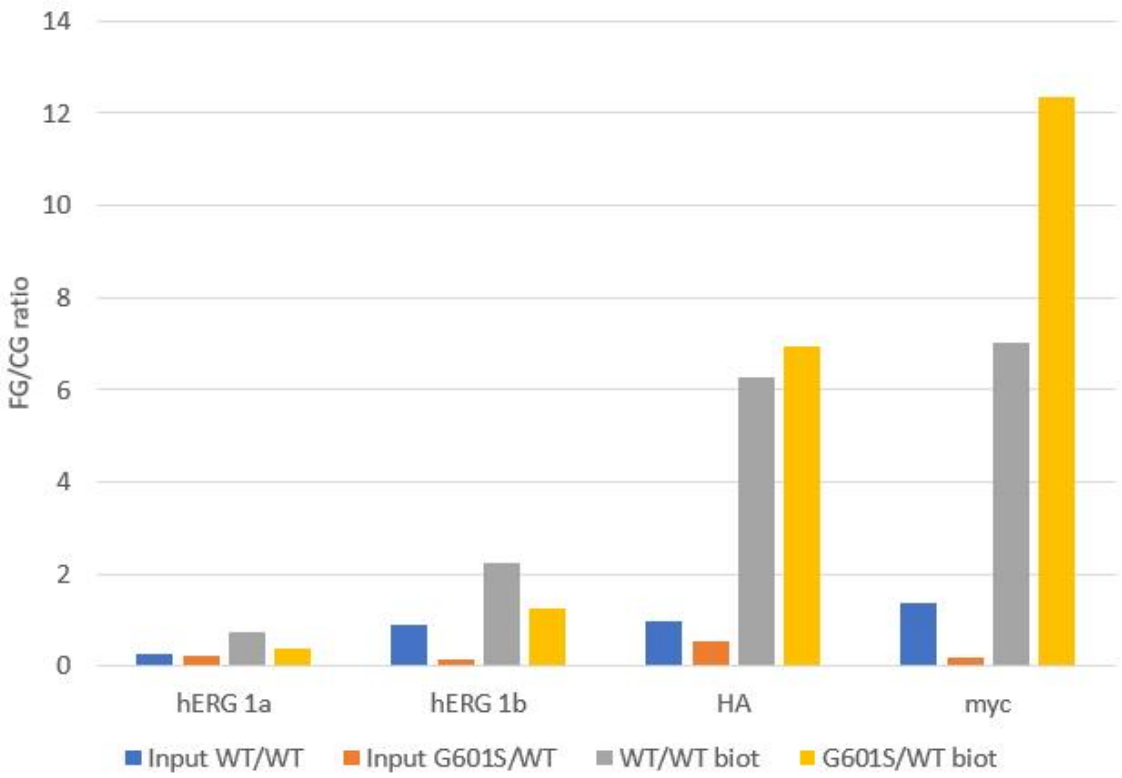
14
12
10
8
6
4
2
0
FG/CG ratio
hERG 1a
hERG 1b
HA
myc
Input WT/WT
Input G601S/WT
WT/WT biot
G601S/WT biot

b

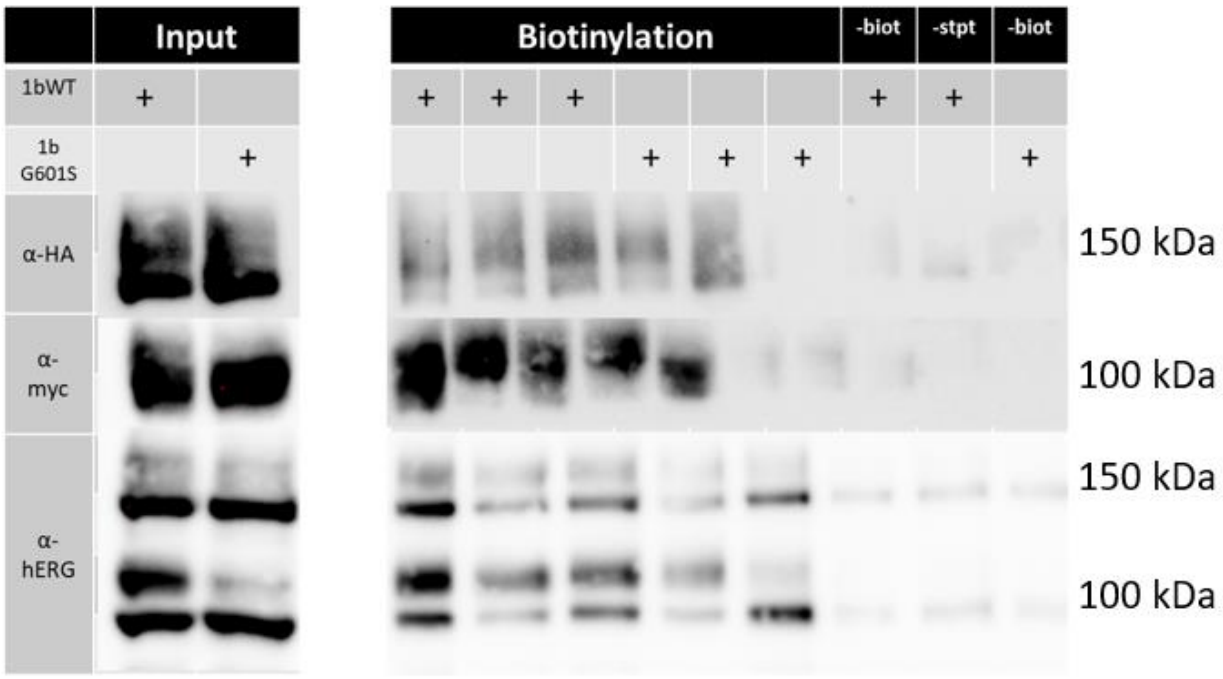
Input
Biotinylation
-biot
-stpt
-biot
1bWT
1b G601S
α-HA
α-myc
α-hERG
150 kDa
100 kDa
150 kDa
100 kDa

Figure 10: Surface biotinylation of hERG in HEK-293 stable cell lines. Cell lines were made stably expressing a bicistronic sequence with both hERG-1b-myc and hERG-1a-HA. For this experiment, 1bWT/1aWT was compared with 1bG601S/1aWT, as other cell lines were not yet available. Sulfo-NHS-SS-biotin was incubated with the cells before lysis. Then, biotinylated protein in lysates was bound to streptavidin-agarose beads and eluate was used for immunoblotting. HA, myc and hERG antibodies were used. (a) demonstrates the enrichment of FG in the biotinylation condition (biot) by comparing the ratio of FG to CG expression. (b) shows the images of the western blots and the controls. "-biot" indicates a condition where no biotin was added, and "-strpt" a condition where no streptavidin was added. Approximate molecular weights are indicated on the right.

Due to limitations in the cloning of hERG noted above, repetitions of the experiments in Figures 6, 7 and 8 with other mutant constructs were not possible. Hence, only 1bWT-myc/1aWT-HA and 1bG601Smyc/1aWTHA were available for sufficient time to be used extensively in this thesis. Despite this setback, the above data demonstrates the feasibility of using the bicistronic hERG HEK-293 Flp-In TREx cells.

Discussion

The misfolding and improper trafficking of hERG has long been known to be the main cause of LQT2. However, previous studies neglected to characterize heteromeric hERG variants, giving an incomplete picture of how the disease presents itself in patients. In this study, co-expression system was developed for the assessment of hERG LQT2-causing mutants in a heteromeric form. It was established that transient co-transfections are not sufficient to compare mutants, and that the stable Flp-In TREx system in HEK-293 cells provide a more robust approach.

Some information can be gleaned from the transient transfections, shown in Figure 6. Notably, 1b-WT maturation was lower than 1a-WT when co-expressed with either mutant. This result is consistent with previous studies showing hERG-1b does not mature well on its own (47). The expression of the mutant I tself did not change significantly whether it was co-expressed with 1a-WT or 1b-WT. As noted in the figure legend, the apparent difference of FG expression between 1a and 1b on the hERG blots can be attributed to the overlap of both 1a signals and does not signify a difference in expression between the two conditions.

The lack of consistency in the transient transfection experiments (Figures 5 and 6) could be explained by a combination of two factors: first, the low transfection efficiency meant very

few cells expressed the genes in the transfected DNA. Consequently, variations in handling and processing (which is more of an absolute error) had a more significant impact than if the baseline expression was higher. The low transfection efficiency was likely a result of two very large plasmids being transfected together (81). Since there were two separate plasmids, it was not possible to guarantee that equal amounts of each were being taken up by each cell. This added a further layer of noise to each condition.

Since making the stable cell lines did not require high transfection efficiency, merely enough that a handful of DNA constructs integrate to the genome, the size of the hERG gene was no longer a factor in lowering final expression levels. As such, we were able to achieve consistent expression. Every cell was expressing one copy each of hERG 1a and hERG 1b.

A major setback with the bicistronic constructs was that we only had the WT and one mutant cell line ready for most of the work due to the difficulty in synthesizing/cloning the DNA. hERG has a very high GC content and many repetitive regions. Furthermore, the bicistronic DNA construct was extremely large (on the order of 12 kDa) and site directed mutagenesis could not be accomplished in this plasmid due to its bicistronic nature (two sites would be mutated). Cutting and pasting hERG out and in was necessary for mutagenesis. The direct cut/paste mechanism proved near impossible, and with TopGene technologies, we developed a strategy to introduce a silent mutation generating a BssHII restriction site in hERG, allowing it to be cloned in two distinct portions. Codons were also optimized to lower the GC content where possible.

Because of these cloning issues, it has not been possible thus far to properly determine whether the cell lines can statistically significantly determine differences between mutants.

However, in the data available to compare mutants, notable differences are detected (Figure 7). Noise between replicates was also noted to be much reduced, and the signal intensities on the blots was quite consistent. More DNA constructs are being produced, meaning more cell lines can be made and experimented on in the future to better assess the differences.

Although the scope of the work comparing different mutants was limited, some key pieces of information can be gleaned from it. The hERG G601S and F805C mutants primarily exhibit their effect by reducing maturation of the WT (and not expressing as well themselves). In Figure 7, the mutants did not reduce expression of the wild-type FG hERG by more than 20%. It was seen that across most conditions the immature core glycosylated hERG remains consistent. The F805C mutant itself is enriched up to 4-fold in its CG form, suggesting it is accumulating in that state and not maturing. On the hERG blot, very little F805C FG band is present, however this is contradicted by the HA blot. The literature indicates that hERG-1b does not mature well on its own, so we would have expected hERG-1b not to mature well with hERG-1a mutants (47). Once again, the mutants in their 1a form would be important as a comparison point for determining whether there is a difference *between* mutants.

Some 1b-specific mutations have been shown to have a dominant negative effect. For example, Jones et al. found 1b-R25W in the N-terminal region of 1b reduced expression of the WT 1a channel (18).

The final WT/G601S and WT/F805C constructs were received from the company weeks before the writing of this thesis, therefore there was inadequate time to assess them extensively.

Hence, more work should be done on the cell lines that have been produced to further assess differences between the mutants.

The stronger co-localization of mutant hERG with the ER marker protein seen in Figure 8 corresponds with the existing literature that hERG quality control primarily takes place in the ER, and that misfolded nascent hERG would remain there until properly folded or degraded. The increased co-localization in the Golgi, however, is less obvious to explain. The marker protein is specifically beta-1,4-galactosyltransferase, which is localized to the Golgi membrane. Given that the G601S mutation is located in proximity to the primary glycosylation sites (N598 and N629), it is possible that the misfolding in this region slows or hinders the glycosylation process. This would increase dwell-time in the Golgi apparatus and potentially increase co-localization signal. Other mutants in different hERG regions should be studied to determine if this is G601S-specific. Differences in signal intensity due to lower mutant expression, and across subcellular locations could be considered. For the plasma membrane, a more appropriate marker, such as mCherry Farnesyl-5 (farnesylation signal) would likely improve the signal intensity. The weak signal observed was likely due to the size of the CFTR marker (180 kDa including the tag), which was chosen only because it was already in our possession.

Co-immunoprecipitation of the 1b-WT/1a-WT and 1b-G601S/1a-WT combinations showed enrichment of the mature FG band (measured by the ratio) in the WT, but not the mutant condition (Figure 9). The degree of enrichment increases from the input to the co-immunoprecipitation condition for the WT. Notably, we see that 1b-WT associates preferentially with 1a-WT in the mature form, as would be expected. In the 1b-G601S condition, very little FG hERG is seen, and no preference for association between FG or CG is observed.

To further validate the co-immunoprecipitation technique, it would have to be performed on at least one additional mutant, particularly one in which we suspect a haploinsufficient mechanism, such as F805C.

The biotinylation experiment seen in Figure 10 confirmed that the cell-surface hERG was primarily the FG form, as expected given previous data. Some CG bands showed up on the biotinylated fraction, albeit significantly less than in the input. This may be a result of the washes during the protocol disrupting the cellular membrane and allowing the biotin to label some intracellular protein. Incomplete quenching could also have resulted in some biotin reacting with intracellular proteins post-lysis.

Certain variability is visible when comparing hERG-blots to HA or myc immunoblots even when looking at the same sample. This is a common issue in immunoblotting and is one reason why they are typically used more in a semi-quantitative manner. In particular, the binding site of the antibodies is different, with the HA and myc antibodies binding the tag inserted within the S1/S2 linker. On the other hand, the hERG antibody is polyclonal and raised against the C-terminus. As a result, the antibodies can have different binding kinetics, thus increases/decreases in expression may appear as different relative changes on a blot. At high and low protein concentrations, antibody binding may not follow a linear pattern. When linear, the slope of band intensity versus amount of protein may not be the same across data. We tested this and found that the HA/myc blots had 1.5-2-fold larger slope than the hERG blot within our working concentration range for the transient transfections. As a result, differences observed on the HA/myc blot would be expected to be more extreme. Normalizing to such a standard curve would

be of use if absolute changes in protein expression need to be measured. In our case, the relative change between mutants was sufficient.

Taken together, the immunoblots, co-immunoprecipitation, and biotinylation demonstrate a reduction in WT hERG level when co-expressed with the G601S mutant. This is consistent with the dominant negative mechanism it was hypothesized to have.

Although the HEK-293 cells represent a flexible and robust technique for performing hERG assays, their applicability to hERG in a cardiac context has limitations. HEK-293 cells do not express all the signalling and regulatory factors that would be found in cardiomyocytes. Similarly, the translational regulation and alternative splicing is not accomplished on a transgene as used here. We only express one version of hERG-1a and one version of hERG-1b, whereas *in vivo*, both hERG 1a and 1b are present in their WT and mutant forms.

Induced pluripotent stem-cell derived cardiomyocytes (iPSC-CM's) present an opportunity to study the mutants in their native setting, and our lab is in the early stages of working with them. The mutations and tags can be edited into the genome of the SC's with CRISPR-Cas9 and the cells can be differentiated to cardiomyocytes. Although this work is significantly more laborious and expensive, the data from it more strongly supports the clinical relevance of data relating to the mutations. The optimal solution is to combine both techniques: the HEK-293 cells should be used to explore a wider range of mutants with a broader set of techniques. When significant evidence of a mutant's disease-causing nature is found, iPSC lines can be made and used to validate the results.

Initial pilot experiments we did transfecting hERG-1b alone showed that an FG band was produced, contradicting some data in the literature. Very recently, it was discovered that hERG channels with the PAS domain deleted can have other PAS domains applied in trans (61). This could suggest that other PAS domains may stand in for the hERG-1a PAS domains, slowing closing time. Furthermore, regulation by other PAS-domain containing proteins may be a contributing factor to why maturation levels appear different across cell lines, as the association of hERG channels in lipid rafts on the cell surface may help keep them stable on the cell surface.

Other types of experiments should be conducted on the stable cell lines. First and foremost, would be evaluating their electrophysiological characteristics by patch clamp. The claim that the heteromeric channels better represent physiological conditions is based on the literature, but that needs to be assessed firsthand. Likewise, observing the correlation between the electrophysiological phenotype and the maturation observed by immunoblotting would confirm their correlation. Native-PAGE should be performed to determine the stoichiometry of hERG across mutant combinations. The different molecular weights of hERG-1a and hERG-1b provide a simple method to determine this. Cell-surface ELISA (measuring signal from antibody on unpermeabilized cells) would help support the data from biotinylation techniques, assessing the amount of hERG on the cell surface. These techniques were attempted but did not reach a usable state in time for the writing of this thesis.

Once the range of techniques are optimized, a larger library of mutants should be tested to assess whether there is a correlation on mutation type/location and the resultant phenotype. This data would then be useful to determining how a patient with a given mutation should be treated.

Conclusion and Summary

In this work, we compared two systems for studying LQT2 causing mutations in heteromeric hERG 1a and 1b channels. The first was transient transfection of HeLa cells. After this method proved to not be reproducible, a second method was developed using stably transfected HEK-293 Flp-In TREx cells. These systems were validated by comparing two mutants known to exhibit haploinsufficient (F805C) or dominant negative (G601S) mechanisms. The Flp-In TREx method consistently showed a reduction in WT expression when co-expressed with the G601S mutant, supporting its dominant negative mechanism. For the F805C mutant, it was observed to accumulate in its immature form, although more work should be done to assess its effect on WT hERG.

These findings demonstrate the feasibility of performing these in-depth assays on a wider range of hERG mutants, with the eventual goal of using such a data set to treat patients depending on their hERG mutation profile.

Materials and Methods

Cell culture

Flp-In™ TREX Hek-293 cells (Invitrogen, from David Thomas' lab) were used for the majority of experiments, stable cell lines were generated as described in **Generation of stable FlpIn TREx 293 cell lines**. HeLa cells were used for pilot experiments where indicated. All cells were grown in Dulbecco's Modified Eagle's Medium (DMEM) with added 10% fetal bovine serum, 100 units/mL penicillin and 100μg/mL streptomycin (mixture referred to as DMEM(+)). All cell culture media were purchased from Wisent. Cells were incubated at 37°C with 5% CO_2.

Creation of hERG(S1-S2 HA) and hERG(S1-S2 myc) DNA constructs

WT, G601S and F805C hERG-1a with an HA (YPYDVPDYA) tag between the S1 and S2 helices (after amino acid 433) in pcDNA3.1 vectors were gifted by Eckard Ficker. Corresponding hERG-1a myc and hERG-1b HA and myc constructs were made with the tags in the same position by Bio Basic Inc. using their gene synthesis service.

Creation of bicistronic hERG constructs

A bicistronic vector containing hERG1a-FLAG and hERG1a-HA (N-terminal) was gifted by Jaime Vandenberg. The first position was flanked by HindIII and BamHI, followed by an IRES, and a second position flanked by EcoRV and NotI. Starting from this, hERG-1b (S1-S2 myc) and hERG-1a (S1-S2 HA) were inserted to the first and second positions, respectively. These steps were completed by both Bio Basic Inc. and TopGene technologies. Several mutant combinations were made, listed in the table below.

Table II: Bicistronic hERG constructs made for this study and their abbreviations.

Short name	hERG-1b (S1-S2 myc)	hERG-1a (S1-S2 HA)
WT/WT	Wild-type	Wild-type
G601S/WT	G601S (pore domain)	Wild-type
WT/G601S	Wild-type	G601S (pore domain)
F805C/WT	F805C (CNBHD)	Wild-type
WT/F805C	Wild-type	F805C (CNBHD)
WT/F29L	Wild-type	F29L (PAS)
WT/T65P	Wild-type	T65P (PAS)
WT/A78P	Wild-type	A78P (PAS

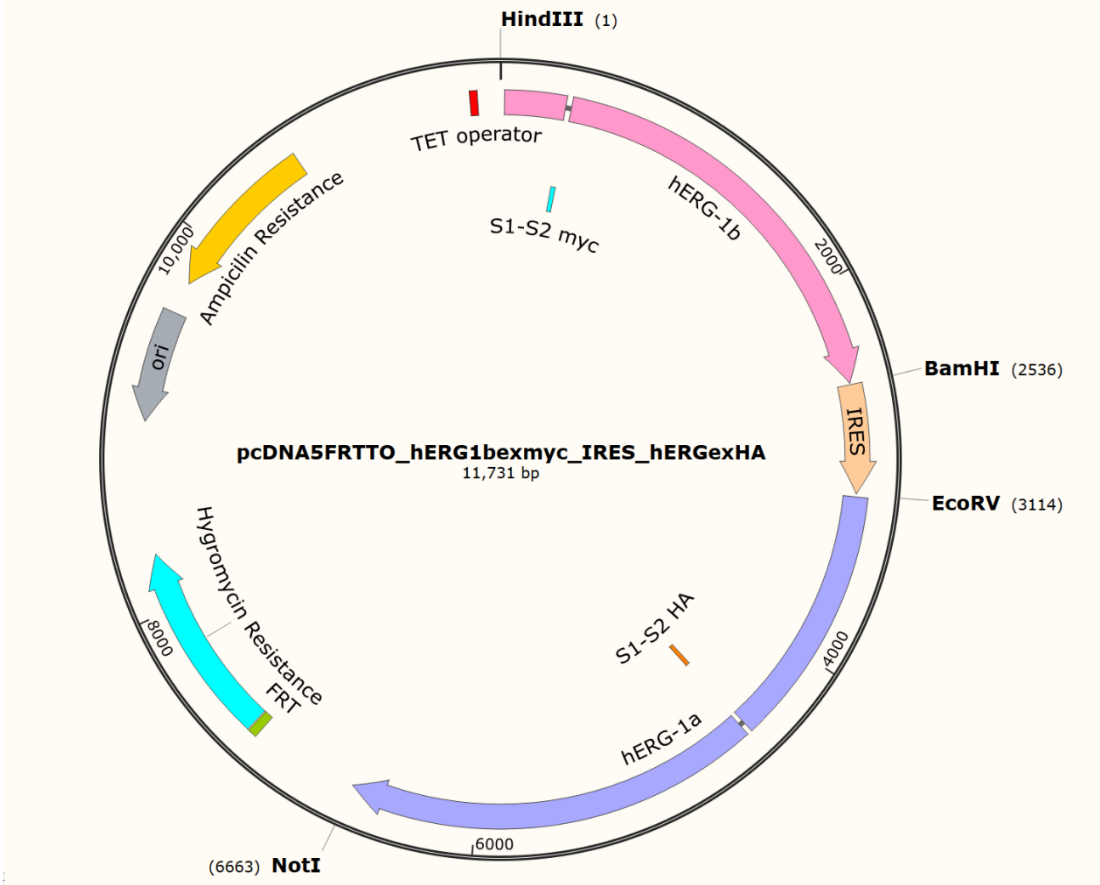

Figure 11: Map of wild-type/wild-type pcDNA5 FRT/TO hERG1b(ex-myc)_IRES_hERG1a(ex-HA) plasmid. Using previously made S1-S2 tagged hERG constructs, hERG-1b with a myc tag and hERG-1a with a HA tag were inserted to a bicistronic vector containing an IRES. This vector also contains a flippase recognition target (FRT) site to enable recombination in stable HEK-293 Flp-In TREx cell lines. Map created with SnapGene software (www.snapgene.com).

Transient Transfections

a. HeLa cells

$1.5*10^4$ cells/mL were plated in desired dish size (6-well plate (6WP) with 2 mL for immunoblotting) one day before transfection. Subsequently, 2 ug total DNA (for 6WP) was mixed with 3 uL Fugene 6 transfection reagent (ProMega) and left for 15 minutes. The media on the cells was changed to DMEM with FBS but not antibiotics. The DNA:transfection reagent mixture was pipetted onto the cells and left for 5 hours. Afterwards, the cells were split at a ratio of 1:2. Cells were used for subsequent experiments approximately 48 hours after transfection.

b. Flp-In TREx HEK-293 cells

$1.2*10^5$ cells/mL were plated in desired dish size (6WP with 2 mL for microscopy) one day before transfection. Subsequently, 2 ug total DNA (for 6WP) was mixed with 3 uL Fugene 6 transfection reagent (ProMega) and left for 15 minutes. The media on the cells was changed to DMEM with FBS but not antibiotics. The DNA:transfection reagent mixture was pipetted onto the cells and left for 5 hours before being replaced with DMEM+. Cells were used for experiments approximately 48 hours after transfection.

Generation of stable FlpIn TREx 293 cell lines

6 µg of each pcDNA5/FRT/TO bicistronic hERG construct was co-transfected with 0.6 µg pOG44 (or pcDNA3.1 for recombination control) to FlpIn TREx cells in 90% confluent 100mm dishes using Fugene 6 transfection reagent. Medium containing DNA and transfection reagent was replaced after 5 hours.

48 hours later, each cell treatment was split into 3x100 mm dishes and incubated in 10 mL 200 μg/mL Hygromycin B until foci developed (approx. 3 weeks), with medium changes twice per week. Cells were then trypsinized, and tested for hERG expression (immunoblotting) and Zeocin (100 μg/mL) sensitivity.

Induction of hERG expression in FlpIn TREx 293 cell lines

Cell were seeded in appropriate plates at a concentration of $0.15x10^5$ cells/mL. The following day, media was replaced with DMEM-(+) containing 10 ng/mL doxycycline (unless otherwise stated) and left for 24 hours. After which, the media was removed and experimental treatments were conducted.

Immunoprecipitation

HA or myc tagged hERG expression was induced (by doxycycline or transfection), and lysates were prepared in 0.1% Triton X-100/ phosphate-buffered saline (PBS). Upon equalization of protein concentrarion using Pierce™ BCA Protein Assay Kit (Thermo Scientific) to roughly 2 mg/mL, lysate was mixed with 20 uL Pierce™ Anti-HA or Anti-myc Magnetic Beads (cat. 88836 or 88842, respectively. Lysates and beads were incubated shaking at room temperature for 30 minutes, then eluted in Lamelli Loading Buffer (LLB) without β-mercaptoethanol at 70˚C for 10 minutes. Eluates were used for immunoblotting (see **Immunoblotting**).

Surface Biotinylation

2 mL EZ-Link™ Sulfo-NHS-SS-Biotin (Thermo-Fisher) in 0.8 mM solution with PBS++ (PBS with 0.9 mM $CaCl_2$ and 0.5 mM $MgCl_2$) was added to live cells and incubated for 10 minutes at room temperature. The biotinylation reaction was then quenched in 1 mL quenching buffer (50 mM Tris pH 8.0), and lysates were subsequently prepared in 1% Triton X-100/PBS. Lysates were

diluted to equal concentration (roughly 2 mg/mL total protein) and incubated with 30 uL Streptavidin agarose beads shaking at room temperature for 1 hour. Afterwards, protein was eluted from the beads at 70 ˚C in 1X LLB (with β-mercaptoethanol) for 10 minutes. Eluates were subsequently used for immunoblotting (see **Immunoblotting**).

Immunoblotting

Protein concentration of lysates was measured using Pierce™ BCA Protein Assay Kit (Thermo Scientific). Equal amounts of protein (~20 μg) were mixed with 2X Lamelli Loading Buffer (LLB), heated to 65°C for 5 minutes, and separated by SDS-PAGE on 7% polyacrylamide gels at 200V for 45 minutes. LLB was prepared without reducing agent, and β-mercaptoethanol was added before heating samples. Proteins were transferred to a 0.45 μm nitrocellulose membrane (Amersham) using a Bio-Rad Trans-Blot® Transfer Cell, at 0.05 A/gel overnight. Membranes were blocked in PBS/5% milk for 60 minutes before incubation in primary antibody solution (PBS/5% milk) for 2 hours at 22°C or 16 hours at 4°C, 3x10 minute PBS/0.1% Triton-X-100 washes, followed by 2 hour 22°C in secondary antibody solution (PBS/5% milk). Antibodies are indicated in **Antibodies** section. Chemiluminescence signals were detected with Amersham ECL Prime Western Blotting Detection Reagent using a Bio-Rad ChemiDoc™ Imaging system. Images were analyzed by densitometry with Bio-Rad Image Lab™ software.

Microscopy and Immunostaining

Cells were grown on coverslips treated with poly-D-lysine in 6-well plates, induced with doxycycline and/or transfected (see other sections). Cells were then fixed for 10 minutes in 4%paraformaldehyde/PBS (electron microscopy sciences), permeabilized in 0.1% TX-100/PBS for 10 minutes, blocked in 5% Bovine Serum Albumin (BSA)/PBS for 30 minutes, incubated in primary

antibodies (Table) shaking for 2 hours, then for 1 hour in secondary antibody (see **Antibodies**) shaking. Finally, cells were stained with 0.3 uM DAPI in PBS. Coverslips were mounted using ProLong Glass Antifade Mountant (Thermo Fisher) and dried at room temperature for 24 hours. Afterwards, slides were stored in the dark at 4°C.

Microscope slides were observed with a Zeiss AxioObserver Z1 microscope (regular images) with a X-Cite Series 12Q lamp on the 63X objective with DAPI, Texas Red and GFP filters. Images were captured using a Zeiss Axiocam MR3 and the Zeiss Axiovision 4.8 software. Confocal microscope images were acquired on a Zeiss LSM 710 laser scanning microscope.

Co-localization Microscopy Experiments

In co-localization experiments, cells were treated as described in **Microscopy and Immunostaining**, but were transfected (see **Transient Transfection** section) with mCherry Golgi 7 (AddGene plasmid #55052), mCherry-ER-3 (AddGene plasmid #55041), mCherry-Endo-14 AddGene plasmid #55040) and mCherry-Lyosomes-20 (AddGene plasmid #55073). All were gifts from Michael Davidson. For the plasma membrane labelling, pcDNA-wt-CFTR-mCherry was used, a gift from Gergely Lukacs.

Antibodies

Primary antibodies and their dilutions are indicated in Table III.

Table III: Primary antibodies used for immunostaining and immunoblotting.

Antibody (α)	Manufacturer	Cat #	Dilution (IB)	Dilution (IF)
HA	Biolegend	901514	1/1000	1/500
Myc	BioXCell	BE0238-1MG-A	Variable, 100 ug used	N/A
hERG	Alomone labs	APC-062	1/2000	N/A
Tubulin	Sigma-Aldrich	T9026	1/10000	N/A

Secondary antibodies were α-mouse or α-rabbit HRP (Jackson Immunoresearch) for immunoblotting (1:10000 dilution) and Alexa 488 goat α-mouse (1:1000 dilution, Invitrogen # A-11029) for immunostaining.

References

1. Smolderen, K. G., Bell, A., Lei, Y., Cohen, E. A., Steg, P. G., Bhatt, D. L., Mahoney, E. M., and investigators, R. r. (2010) One-year costs associated with cardiovascular disease in Canada: Insights from the REduction of Atherothrombosis for Continued Health (REACH) registry. *Can J Cardiol* **26**, 297-305

2. Duvall, W. L. (2003) Cardiovascular disease in women. *Mt Sinai J Med* **70**, 293-305

3. Koeppen, B. M., and Stanton, B. A. (2018) *Berne & Levy physiology*, Seventh edition. ed., Elsevier, Philadelphia, PA

4. Stracina, T., Ronzhina, M., Redina, R., and Novakova, M. (2022) Golden Standard or Obsolete Method? Review of ECG Applications in Clinical and Experimental Context. *Front Physiol* **13**, 867033

5. Roberge, F. A., Nadeau, R. A., and James, T. N. (1968) The nature of the PR interval. *Cardiovasc Res* **2**, 19-30

6. Wahler, G. M. (2001) 52 - Cardiac Action Potentials. in *Cell Physiology Source Book (Third Edition)* (Sperelakis, N. ed.), Academic Press, San Diego. pp 887-898

7. Shih, H. T. (1994) Anatomy of the action potential in the heart. *Tex Heart Inst J* **21**, 30-41

8. Luz, E. J., Schwartz, W. R., Camara-Chavez, G., and Menotti, D. (2016) ECG-based heartbeat classification for arrhythmia detection: A survey. *Comput Methods Programs Biomed* **127**, 144-164

9. Zareba, W., and Cygankiewicz, I. (2008) Long QT syndrome and short QT syndrome. *Prog Cardiovasc Dis* **51**, 264-278

10. Kramer, D. B., and Zimetbaum, P. J. (2011) Long-QT syndrome. *Cardiol Rev* **19**, 217-225

11. Vandenberg, J. I., Perry, M. D., Perrin, M. J., Mann, S. A., Ke, Y., and Hill, A. P. (2012) hERG K(+) channels: structure, function, and clinical significance. *Physiol Rev* **92**, 1393-1478

12. Brenyo, A. J., Huang, D. T., and Aktas, M. K. (2012) Congenital long and short QT syndromes. *Cardiology* **122**, 237-247

13. Schwartz, P. J., Crotti, L., and Insolia, R. (2012) Long-QT syndrome: from genetics to management. *Circ Arrhythm Electrophysiol* **5**, 868-877

14. Yang, T., and Roden, D. M. (1996) Extracellular potassium modulation of drug block of IKr. Implications for torsade de pointes and reverse use-dependence. *Circulation* **93**, 407-411

15. Hedley, P. L., Jorgensen, P., Schlamowitz, S., Wangari, R., Moolman-Smook, J., Brink, P. A., Kanters, J. K., Corfield, V. A., and Christiansen, M. (2009) The genetic basis of long QT and short QT syndromes: a mutation update. *Hum Mutat* **30**, 1486-1511

16. Tester, D. J., Will, M. L., Haglund, C. M., and Ackerman, M. J. (2005) Compendium of cardiac channel mutations in 541 consecutive unrelated patients referred for long QT syndrome genetic testing. *Heart Rhythm* **2**, 507-517

17. Yang, Y., Lv, T. T., Li, S. Y., and Zhang, P. (2021) Sodium channel blockers in the management of long QT syndrome types 3 and 2: A system review and meta-analysis. *J Cardiovasc Electrophysiol* **32**, 3057-3067

18. Jones, D. K., Liu, F., Dombrowski, N., Joshi, S., and Robertson, G. A. (2016) Dominant negative consequences of a hERG 1b-specific mutation associated with intrauterine fetal death. *Prog Biophys Mol Biol* **120**, 67-76

19. Ng, C. A., Perry, M. D., Liang, W., Smith, N. J., Foo, B., Shrier, A., Lukacs, G. L., Hill, A. P., and Vandenberg, J. I. (2020) High-throughput phenotyping of heteromeric human ether-a-go-go-related gene potassium channel variants can discriminate pathogenic from rare benign variants. *Heart Rhythm* **17**, 492-500

20. Ng, C. A., Ullah, R., Farr, J., Hill, A. P., Kozek, K. A., Vanags, L. R., Mitchell, D. W., Kroncke, B. M., and Vandenberg, J. I. (2022) A massively parallel assay accurately discriminates between functionally normal and abnormal variants in a hotspot domain of KCNH2. *Am J Hum Genet* **109**, 1208-1216

21. Jenewein, T., Kanner, S. A., Bauer, D., Hertel, B., Colecraft, H. M., Moroni, A., Thiel, G., and Kauferstein, S. (2020) The mutation L69P in the PAS domain of the hERG potassium channel results in LQTS by trafficking deficiency. *Channels (Austin)* **14**, 163-174

22. Gu, K., Qian, D. D., Qin, H. Y., Cui, C., Fernando, W. C. H. A., Wang, D. W., Wang, J. J., Cao, K. J., and Chen, M. L. (2021) A novel mutation in KCNH2 yields loss-of-function of hERG potassium channel in long QT syndrome 2. *Pflug Arch Eur J Phy* **473**, 219-229

23. Li, C. L., Hu, D. Y., Liu, W. L., Qi, S. Y., Wang, H. T., Li, L., Gong, Q. M., and Zhou, Z. F. (2007) [The mechanistic rote of KCNH2 gene L413P and L559H mutations in long QT syndrome]. *Zhonghua Nei Ke Za Zhi* **46**, 838-841

24. Balijepalli, S. Y., Lim, E., Concannon, S. P., Chew, C. L., Holzem, K. E., Tester, D. J., Ackerman, M. J., Delisle, B. P., Balijepalli, R. C., and January, C. T. (2012) Mechanism of loss of Kv11.1 K+ current in mutant T421M-Kv11.1-expressing rat ventricular myocytes: interaction of trafficking and gating. *Circulation* **126**, 2809-2818

25. Anderson, C. L., Delisle, B. P., Anson, B. D., Kilby, J. A., Will, M. L., Tester, D. J., Gong, Q. M., Zhou, Z. F., Ackerman, M. J., and January, C. T. (2006) Most LQT2 mutations reduce

Kv11.1 (hERG) current by a class 2 (trafficking-deficient) mechanism. *Circulation* **113**, 365-373

26. Yang, H. T., Sun, C. F., Cui, C. C., Xue, X. L., Zhang, A. F., Li, H. B., Wang, D. Q., and Shu, J. (2009) HERG-F463L POTASSIUM CHANNELS LINKED TO LONG QT SYNDROME REDUCE I-Kr CURRENT BY A TRAFFICKING-DEFICIENT MECHANISM. *Clin Exp Pharmacol P* **36**, 822-827

27. Gong, Q. M., Anderson, C. L., January, C. T., and Zhou, Z. F. (2004) Pharmacological rescue of trafficking defective HERG channels formed by coassembly of wild-type and long QT mutant N470D subunits. *Am J Physiol-Heart C* **287**, H652-H658

28. Liu, L., Hayashi, K., Kaneda, T., Ino, H., Fujino, N., Uchiyama, K., Konno, T., Tsuda, T., Kawashiri, M. A., Ueda, K., Higashikata, T., Shuai, W., Kupershmidt, S., Higashida, H., and Yamagishi, M. (2013) A novel mutation in the transmembrane nonpore region of the KCNH2 gene causes severe clinical manifestations of long QT syndrome. *Heart Rhythm* **10**, 61-67

29. Nakajima, T., Furukawa, T., Tanaka, T., Katayama, Y., Nagai, R., Nakamura, Y., and Hiraoka, M. (1998) Novel mechanism of HERG current suppression in LQT2: shift in voltage dependence of HERG inactivation. *Circ Res* **83**, 415-422

30. Kinoshita, K., Yamaguchi, Y., Nishide, K., Kimoto, K., Nonobe, Y., Fujita, A., Asano, K., Tabata, T., Mori, H., Inoue, H., Hata, Y., Fukurotani, K., and Nishida, N. (2012) A novel missense mutation causing a G487R substitution in the S2-S3 loop of human ether-a-go-go-related gene channel. *J Cardiovasc Electrophysiol* **23**, 1246-1253

31. Amin, A. S., Herfst, L. J., Delisle, B. P., Klemens, C. A., Rook, M. B., Bezzina, C. R., Underkofler, H. A., Holzem, K. M., Ruijter, J. M., Tan, H. L., January, C. T., and Wilde, A. A. (2008) Fever-induced QTc prolongation and ventricular arrhythmias in individuals with type 2 congenital long QT syndrome. *J Clin Invest* **118**, 2552-2561

32. Li, C.-l., Hu, D.-y., Liu, W.-l., Qi, S.-y., Wang, H.-t., Li, L., Gong, Q.-m., and Zhou, Z.-f. (2007) [The mechanistic rote of KCNH2 gene L413P and L559H mutations in long QT syndrome]. *Zhonghua nei ke za zhi* **46**, 838-841

33. Sanguinetti, M. C., Curran, M. E., Spector, P. S., and Keating, M. T. (1996) Spectrum of HERG K+-channel dysfunction in an inherited cardiac arrhythmia. *Proc Natl Acad Sci U S A* **93**, 2208-2212

34. ZHAO, J. T., HILL, A. P., VARGHESE, A., COOPER, A. A., SWAN, H., LAITINEN-FORSBLOM, P. J., REES, M. I., SKINNER, J. R., CAMPBELL, T. J., and VANDENBERG, J. I. (2009) Not All hERG Pore Domain Mutations Have a Severe Phenotype: G584S Has an Inactivation Gating Defect with Mild Phenotype Compared to G572S, Which Has a Dominant

Negative Trafficking Defect and a Severe Phenotype. *Journal of Cardiovascular Electrophysiology* **20**, 923-930

35. Keller, S. H., Platoshyn, O., and Yuan, J. X. (2005) Long QT syndrome-associated I593R mutation in HERG potassium channel activates ER stress pathways. *Cell Biochem Biophys* **43**, 365-377

36. Huo, J., Zhang, Y., Huang, N., Liu, P., Huang, C., Guo, X., Jiang, W., Zhou, N., Grace, A., Huang, C. L., and Ma, A. (2008) The G604S-hERG mutation alters the biophysical properties and exerts a dominant-negative effect on expression of hERG channels in HEK293 cells. *Pflugers Arch* **456**, 917-928

37. Mao, H., Lu, X., Karush, J. M., Huang, X., Yang, X., Ba, Y., Wang, Y., Liu, N., Zhou, J., and Lian, J. (2013) Pharmacologic Approach to Defective Protein Trafficking in the E637K-hERG Mutant with PD-118057 and Thapsigargin. *Plos One* **8**, e65481

38. Gong, Q., Keeney, D. R., Robinson, J. C., and Zhou, Z. (2004) Defective assembly and trafficking of mutant HERG channels with C-terminal truncations in long QT syndrome. *J Mol Cell Cardiol* **37**, 1225-1233

39. Aidery, P., Kisselbach, J., Gaspar, H., Baldea, I., Schweizer, P. A., Becker, R., Katus, H. A., and Thomas, D. (2012) Identification and functional characterization of the novel human ether-a-go-go-related gene (hERG) R744P mutant associated with hereditary long QT syndrome 2. *Biochem Biophys Res Commun* **418**, 830-835

40. Lin, T. F., Wu, H. H., Tang, C. Y., and Jeng, C. J. (2015) The Subfamily-Specific Assembly of Eag and Erg K+ Channels is Determined by Both the Amino and the Carboxyl Recognition Domains. *Biophys J* **108**, 276a-276a

41. Puckerin, A., Aromolaran, K. A., Chang, D. D., Zukin, R. S., Colecraft, H. M., Boutjdir, M., and Aromolaran, A. S. (2016) hERG 1a LQT2 C-terminus truncation mutants display hERG 1b-dependent dominant negative mechanisms. *Heart Rhythm* **13**, 1121-1130

42. Tobert, K. E., Tester, D. J., Zhou, W., Haglund-Turnquist, C. M., Giudicessi, J. R., and Ackerman, M. J. (2022) Genome sequencing in a genetically elusive multigenerational long QT syndrome pedigree identifies a novel LQT2-causative deeply intronic KCNH2 variant. *Heart Rhythm* **19**, 998-1007

43. Abbott, G. W., Sesti, F., Splawski, I., Buck, M. E., Lehmann, W. H., Timothy, K. W., Keating, M. T., and Goldstein, S. A. N. (1999) MiRP1 forms I-Kr potassium channels with HERG and is associated with cardiac arrhythmia. *Cell* **97**, 175-187

44. McNally, B. A., Pendon, Z. D., and Trudeau, M. C. (2017) hERG1a and hERG1b potassium channel subunits directly interact and preferentially form heteromeric channels. *J Biol Chem* **292**, 21548-21557

45. Wang, W., and MacKinnon, R. (2017) Cryo-EM Structure of the Open Human Ether-a-go-go-Related K(+) Channel hERG. *Cell* **169**, 422-430 e410

46. Johnson, A. A., Crawford, T. R., and Trudeau, M. C. (2022) The N-linker region of hERG1a upregulates hERG1b potassium channels. *J Biol Chem* **298**, 102233

47. Phartiyal, P., Sale, H., Jones, E. M., and Robertson, G. A. (2008) Endoplasmic reticulum retention and rescue by heteromeric assembly regulate human ERG 1a/1b surface channel composition. *J Biol Chem* **283**, 3702-3707

48. Subbiah, R. N., Clarke, C. E., Smith, D. J., Zhao, J., Campbell, T. J., and Vandenberg, J. I. (2004) Molecular basis of slow activation of the human ether-a-go-go related gene potassium channel. *J Physiol* **558**, 417-431

49. Codding, S. J., Johnson, A. A., and Trudeau, M. C. (2020) Gating and regulation of KCNH (ERG, EAG, and ELK) channels by intracellular domains. *Channels (Austin)* **14**, 294-309

50. Sun, J., and MacKinnon, R. (2017) Cryo-EM Structure of a KCNQ1/CaM Complex Reveals Insights into Congenital Long QT Syndrome. *Cell* **169**, 1042-+

51. Sanguinetti, M. C., and Tristani-Firouzi, M. (2006) hERG potassium channels and cardiac arrhythmia. *Nature* **440**, 463-469

52. Blass, B. E. (2021) Chapter 14 - Case studies in drug discovery. in *Basic Principles of Drug Discovery and Development (Second Edition)* (Blass, B. E. ed.), Academic Press. pp 625-664

53. Suessbrich, H., Waldegger, S., Lang, F., and Busch, A. E. (1996) Blockade of HERG channels expressed in Xenopus oocytes by the histamine receptor antagonists terfenadine and astemizole. *FEBS Lett* **385**, 77-80

54. Asai, T., Adachi, N., Moriya, T., Oki, H., Maru, T., Kawasaki, M., Suzuki, K., Chen, S., Ishii, R., Yonemori, K., Igaki, S., Yasuda, S., Ogasawara, S., Senda, T., and Murata, T. (2021) Cryo-EM Structure of K(+)-Bound hERG Channel Complexed with the Blocker Astemizole. *Structure* **29**, 203-212 e204

55. Vandenberg, J. I., Perozo, E., and Allen, T. W. (2017) Towards a Structural View of Drug Binding to hERG K(+) Channels. *Trends Pharmacol Sci* **38**, 899-907

56. Gong, Q., Anderson, C. L., January, C. T., and Zhou, Z. (2004) Pharmacological rescue of trafficking defective HERG channels formed by coassembly of wild-type and long QT mutant N470D subunits. *Am J Physiol Heart Circ Physiol* **287**, H652-658

57. Foo, B. (2019) Peripheral quality control of mutant hERG potassium channels: contribution to long-QT syndrome pathogenesis and pharmacological correction.

58. Codding, S. J., and Trudeau, M. C. (2019) The hERG potassium channel intrinsic ligand regulates N- and C-terminal interactions and channel closure. *J Gen Physiol* **151**, 478-488

59. Kratz, J. M., Grienke, U., Scheel, O., Mann, S. A., and Rollinger, J. M. (2017) Natural products modulating the hERG channel: heartaches and hope. *Nat Prod Rep* **34**, 957-980

60. Long, Y., Lin, Z., Xia, M., Zheng, W., and Li, Z. (2013) Mechanism of HERG potassium channel inhibition by tetra-n-octylammonium bromide and benzethonium chloride. *Toxicol Appl Pharmacol* **267**, 155-166

61. Soohoo, S. M., Tiwari, P. B., Suzuki, Y. J., and Brelidze, T. I. (2022) Investigation of PAS and CNBH domain interactions in hERG channels and effects of long-QT syndrome-causing mutations with surface plasmon resonance. *J Biol Chem* **298**, 101433

62. Moglich, A., Ayers, R. A., and Moffat, K. (2009) Structure and signaling mechanism of Per-ARNT-Sim domains. *Structure* **17**, 1282-1294

63. Brelidze, T. I., Gianulis, E. C., DiMaio, F., Trudeau, M. C., and Zagotta, W. N. (2013) Structure of the C-terminal region of an ERG channel and functional implications. *Proc Natl Acad Sci U S A* **110**, 11648-11653

64. Sansom, M. S. (1999) Ion channels: structure of a molecular brake. *Curr Biol* **9**, R173-175

65. Huang, X. P., Mangano, T., Hufeisen, S., Setola, V., and Roth, B. L. (2010) Identification of Human Ether-a-go-go Related Gene Modulators by Three Screening Platforms in an Academic Drug-Discovery Setting. *Assay Drug Dev Techn* **8**, 727-742

66. Butler, A., Helliwell, M. V., Zhang, Y., Hancox, J. C., and Dempsey, C. E. (2019) An Update on the Structure of hERG. *Front Pharmacol* **10**, 1572

67. Apud, J. A., Zhang, F. Y., Decot, H., Bigos, K. L., and Weinberger, D. R. (2012) Genetic Variation in KCNH2 Associated With Expression in the Brain of a Unique hERG Isoform Modulates Treatment Response in Patients With Schizophrenia. *Am J Psychiat* **169**, 725-734

68. Apaja, P. M., Foo, B., Okiyoneda, T., Valinsky, W. C., Barriere, H., Atanasiu, R., Ficker, E., Lukacs, G. L., and Shrier, A. (2013) Ubiquitination-dependent quality control of hERG K+ channel with acquired and inherited conformational defect at the plasma membrane. *Mol Biol Cell* **24**, 3787-3804

69. Mayer, M. P., and Bukau, B. (2005) Hsp70 chaperones: cellular functions and molecular mechanism. *Cell Mol Life Sci* **62**, 670-684

70. Kampinga, H. H., and Craig, E. A. (2010) The HSP70 chaperone machinery: J proteins as drivers of functional specificity. *Nat Rev Mol Cell Biol* **11**, 579-592

71. Roder, K., Kabakov, A., Moshal, K. S., Murphy, K. R., Xie, A., Dudley, S., Turan, N. N., Lu, Y. C., MacRae, C. A., and Koren, G. (2019) Trafficking of the human ether-a-go-go-related gene (hERG) potassium channel is regulated by the ubiquitin ligase rififylin (RFFL). *Journal of Biological Chemistry* **294**, 351-360

72. Zhang, H., Amick, J., Chakravarti, R., Santarriaga, S., Schlanger, S., McGlone, C., Dare, M., Nix, J. C., Scaglione, K. M., Stuehr, D. J., Misra, S., and Page, R. C. (2015) A bipartite interaction between Hsp70 and CHIP regulates ubiquitination of chaperoned client proteins. *Structure* **23**, 472-482

73. Cant, N., Pollock, N., and Ford, R. C. (2014) CFTR structure and cystic fibrosis. *Int J Biochem Cell Biol* **52**, 15-25

74. Baaklini, I., Goncalves, C. C., Lukacs, G. L., and Young, J. C. (2020) Selective Binding of HSC70 and its Co-Chaperones to Structural Hotspots on CFTR. *Sci Rep* **10**, 4176

75. Lopes-Pacheco, M. (2019) CFTR Modulators: The Changing Face of Cystic Fibrosis in the Era of Precision Medicine. *Front Pharmacol* **10**, 1662

76. White, S. M., Constantin, P. E., and Claycomb, W. C. (2004) Cardiac physiology at the cellular level: use of cultured HL-1 cardiomyocytes for studies of cardiac muscle cell structure and function. *Am J Physiol-Heart C* **286**, H823-H829

77. Fus-Kujawa, A., Prus, P., Bajdak-Rusinek, K., Teper, P., Gawron, K., Kowalczuk, A., and Sieron, A. L. (2021) An Overview of Methods and Tools for Transfection of Eukaryotic Cells in vitro. *Front Bioeng Biotechnol* **9**, 701031

78. Shabani, M., Hemmati, S., Hadavi, R., Amirghofran, Z., Jeddi-Tehrani, M., Rabbani, H., and Shokri, F. (2010) Optimization of Gene Transfection in Murine Myeloma Cell Lines using Different Transfection Reagents. *Avicenna J Med Biotechnol* **2**, 123-130

79. Howcroft, T. K., Kirshner, S. L., and Singer, D. S. (1997) Measure of transient transfection efficiency using beta-galactosidase protein. *Anal Biochem* **244**, 22-27

80. Ramezani, M., Khoshhamdam, M., Dehshahri, A., and Malaekeh-Nikouei, B. (2009) The influence of size, lipid composition and bilayer fluidity of cationic liposomes on the transfection efficiency of nanolipoplexes. *Colloids and Surfaces B: Biointerfaces* **72**, 1-5

81. Yin, W., Xiang, P., and Li, Q. (2005) Investigations of the effect of DNA size in transient transfection assay using dual luciferase system. *Anal Biochem* **346**, 289-294

82. Larsen, A. P., and Olesen, S.-P. (2010) Differential expression of hERG1 channel isoforms reproduces properties of native I Kr and modulates cardiac action potential characteristics. *PLoS One* **5**, e9021